



**Difference in soil parameters between disturbed and  
undisturbed permafrost soil in Northwest Territories,  
Canada**

A thesis presented for the degree of Bachelor of Science

at

Institute of Environmental Science and Geography  
University of Potsdam  
Germany

Frieder Tautz  
Präsidentenstr. 73  
16816 Neuruppin  
Matrikel-Nr.: 780602  
frtautz@uni-potsdam.de

Potsdam, October 12, 2020

1st supervisor	Prof. Dr. Guido Grosse Alfred-Wegener-Institut, Polar- und Meeresforschung Telegrafenberg A45-N, 14473 Potsdam
2nd supervisor	Prof. Dr. Julia Boike Alfred-Wegener-Institut, Polar- und Meeresforschung Telegrafenberg A6, 14473 Potsdam

# Contents

<b>List of Figures</b>	<b>iv</b>
<b>List of Tables</b>	<b>v</b>
<b>Acronyms</b>	<b>vi</b>
<b>1 Introduction</b>	<b>1</b>
1.1 Scientific background . . . . .	2
1.1.1 Permafrost distribution and properties . . . . .	2
1.1.2 Permafrost carbon climate feedback . . . . .	3
1.1.3 Thermokarst . . . . .	5
1.1.4 Soil Properties . . . . .	8
1.2 Site description . . . . .	10
1.3 Disturbance categories . . . . .	12
<b>2 Methods</b>	<b>14</b>
2.1 Sample extraction in-situ . . . . .	14
2.2 Active layer and permafrost subsampling . . . . .	16
2.3 Laboratory Analyses . . . . .	18
2.3.1 Biochemistry . . . . .	18
2.3.2 Grain size analysis . . . . .	19
2.3.3 Ice content . . . . .	21
2.3.4 Soil Organic Carbon Content . . . . .	22
2.3.5 Radiocarbon dating . . . . .	22
2.4 Statistical approach . . . . .	23
<b>3 Results</b>	<b>25</b>
3.1 General properties . . . . .	25
3.2 Biochemistry in active layer and permafrost . . . . .	28
3.3 Grain size distribution . . . . .	28
3.4 Disturbance categories . . . . .	29

<b>4 Discussion</b>	<b>33</b>
4.1 General Properties . . . . .	34
4.2 Biochemistry in active layer and permafrost . . . . .	35
4.3 Grain size distribution . . . . .	37
4.4 Disturbance categories . . . . .	37
4.5 Limitations and errors . . . . .	39
<b>5 Conclusion</b>	<b>41</b>
<b>6 Acknowledgment</b>	<b>42</b>
<b>7 Eidesstattliche Erklärung</b>	<b>43</b>
<b>8 Appendix</b>	<b>55</b>

## List of Figures

1	Permafrost carbon cycle (Schuur et al. 2015) . . . . .	4
2	Schematic of retrogressive thaw slumps (Lantuit and Pollard 2005) . . . . .	7
3	Schematic of a non-sorted soil profile (Margesin 2009) . . . . .	9
4	Physiographic subdivision and overview map of study sites . . .	11
5	Examples of sites categorised as disturbed at Lake 6 . . . . .	13
6	High vegetation at disturbed sites at Lake 6 . . . . .	14
7	Examples of sites defined as undisturbed . . . . .	14
8	First pit after drilling the first core at Lake 1 . . . . .	15
9	Coring equipment . . . . .	16
10	Sampling setup in-situ . . . . .	17
11	Cylinder and AL soil samples taken at TVC and Lake 11 respectively . . . . .	17
12	Core obtained at Lake 1 in cooling chamber, AWI . . . . .	18
13	Subsampling for different analyses in cooling chamber . . . . .	19
14	Setup of Rhizon soil moisture sampling, AWI Potsdam . . . . .	21
15	Cryotic processes visible in soil profiles . . . . .	25
16	Comparison between AL and permafrost of biochemical values and CN-ratio . . . . .	29
17	Grain size differentiation over the three depth categories of AL measurements . . . . .	30
18	ALT measurements of disturbed and undisturbed sites . . . . .	31
19	Difference between disturbed and undisturbed sites of biochemical parameters . . . . .	32
20	Grain size distribution . . . . .	33
21	Weight percentage of grains larger than 1 mm not included in the grain size analysis . . . . .	41
A1	General temperature regime of permafrost (French 2013) . . . . .	55
A2	Map of sampling setup at Lake 1 regarding the main data set . .	62
A3	Map of sampling setup at Lake 6 regarding the main data set . .	62
A4	Map of sampling setup at Lake 11 regarding the main data set . .	63

A5	Map of sampling setup at TVC and 1sub3 regarding the main data set . . . . .	63
A6	Map of sampling setup at Lake 12 regarding the main data set .	64
A7	Map of sampling setup at Lake 1 regarding the extended data set with ALT measurements . . . . .	64
A8	Map of sampling setup at Lake 6 regarding the extended data set with ALT measurements . . . . .	65
A9	Map of sampling setup at Lake 11 regarding the extended data set with ALT measurements . . . . .	65
A10	Map of sampling setup at Lake 12 regarding the extended data set with ALT measurements . . . . .	66
A11	Map of sampling setup of vegetation sites regarding the extended data set with ALT measurements . . . . .	66

## List of Tables

1	Rate of mineralisation in regard to TOC/TN-ratio (Walthert et al. 2004) . . . . .	5
2	Radiocarbon age at different sites . . . . .	26
3	Summary of additional measurements - gravimetric and volumetric ice content, wet and dry bulk densities . . . . .	27
4	SOCC values at each sample site . . . . .	32
A1	Biochemical parameters of permafrost core and active layer samples . . . . .	55
A1	Grain size distribution . . . . .	57
A1	Excluded grain fraction >1mm . . . . .	59
A1	Extended data set with ALT measurements . . . . .	60

## Acronyms

CH <sub>3</sub> COOH	Acetic acid is a colourless organic acid with the formula CH <sub>3</sub> COOH.
CH <sub>4</sub>	Methane is an organic gas with the formula CH <sub>4</sub> . It is utilised as a fuel and forms naturally below ground and under the seafloor by biological and geological processes. In the atmosphere, it plays an important role as a Greenhouse Gas.
CO <sub>2</sub>	Carbon dioxide is a colourless gas with the formula CO <sub>2</sub> , naturally occurring in the atmosphere and hydrosphere. It plays a major role as a Greenhouse Gas in the atmosphere where it stores thermal energy and enhances global warming.
H <sub>2</sub> O <sub>2</sub>	Hydrogen peroxide is a chemical compound used as an oxidiser, bleaching agent and antiseptic.
N <sub>2</sub> O	Nitrous oxide, also known as laughing gas, is a chemical molecule with the formula N <sub>2</sub> O. It is commonly used as an anaesthetic in health system. In the atmosphere, it acts as a Greenhouse Gas
<sup>12</sup> C	The carbon-12 isotope is the most abundant isotope of carbon and makes roughly 98% of the carbon on earth. Its amount in organics is used to determine its age with the Radiocarbon dating method.
<sup>13</sup> C	The carbon-13 isotope is one of the three carbon isotope, is quite stable and makes roughly 1 % of the naturally occurring carbon on earth.
<sup>14</sup> C	The carbon-14 isotope is quite unstable and the rarest of all three carbon isotopes. Its occurrence and decay in organic materials is the basis of the Radiocarbon dating method utilised to determine the age of organics.
<sup>14</sup> N	The nitrogen-14 isotope is the major isotope of nitrogen.
m <sup>3</sup>	1 cubic metre = 1m * 1m * 1m.
°C	Degree Celsius is a common unit to describe temperature. Zero degree celsius are 32 Fahreneinheit or 273,15 Kelvin.
14C	Radiocarbon dating is method utilising the decay of the <sup>14</sup> C isotope to determine the age of organic materials for example in soils.
a	years
AL	The Active layer is the top soil layer in permafrost areas. It freezes in winter and thaws in summer due to seasonal changes.
ALT	The Active Layer Thickness is the average annual thaw depth of the active layer.
AMS	The Accelerator Mass Spectrometer is a sensitive device measuring the amount and type of isotopes in a probe. Its major use is to determine Radiocarbon date by measuring the amount of the according isotopes.

AWI	Alfred-Wegener-Institut, Helmholtz-Zentrum for Polar and Marine Research
C	Carbon is a chemical element and the main component of all organics on earth.
C/N ratio	The Total Organic Carbon to Total Nitrogen ration describes the proportion between those two soil components and is often utilised to indicate the rate of mineralisation in the soil (Walthert et al. 2004).
cal. a BP	Calibrated radiocarbon years before present refer to the corrected age calculation of organic material with the Radiocarbon dating method. Due to different concentrations in the past, the age calculations requires adjustment according to the historic isotope concentrations in the atmosphere.
cm	1 centimetre = $1 * 10^{-2}$ m
DZAA	The Depth of Zero Annual Amplitude describes the depth in permafrost soils where there is no annual fluctuations by seasonal changes (<0.1 degree celsius (°C)). It is utilised to determine long-term changes of the permafrost temperature.
g	Gram is the SI-unit for weight.
GHG	Greenhouse Gases are radioactive gases in the thermal infrared spectrum rising global temperatures with rising concentrations in the atmosphere. This process is termed Greenhouse Effect.
GSD	The Grain Size Distribution describes the size and relative amount of grains in a probe by mass or volume. It determines the soil class, the soils composition and movement of water.
ka	Thousand years
kg	1 kilogram = 10 g
kg/m <sup>2</sup>	kilograms per square metre
km	1 kilometre = 1000 m
km <sup>2</sup>	1 square kilometre = 1km * 1km
m	metre (SI-unit of length)
m <sup>2</sup>	1 square metre = 1m * 1m
m/a	metre per year
mg	1 Milligram = $10^{-3}$ metre
mineralisation	Mineralisation is the process of complete decomposition of organic material to inorganic components - mainly by microorganisms activity. It releases primarily photosynthetically sequestered carbon as carbon dioxide as well as other components of the cycle of matter such as nitrogen, phosphor or sulphur.
ml	1 millilitre = $10^{-3}$ litre.
mm	1 Millimetre = $10^{-3}$ metre
N	Nitrogen is a chemical element with the formula N. In soils it is often the limiting nutrient for plants.
North	The decimal latitudinal degrees is a unit to describe a position on earth. Together with the longitudinal degrees, each position on the surface can be assigned to a unique combination of Latitudes and Longitudes. Due to the fact that latitudinal degrees are describing the angle towards the equator, they are divided by their position relative to the equator into north and south.

NWT	The Northwestern Territories is a state north-west in Canada.
OM	Organic Matter is the carbon-based component of a sample which derives from living organisms such as plants, animals and microbes.
Pg	1 Pg = $10^{15}$ g
RCP	The Representatiive Concentration Pathway describes the trajectory of Greenhouse Gases (GHG) concentration in the atmosphere in the future and is utilised for modeling and research purposes. The concentrations are highly dependent on the emissions by human kind.
SOCC	The Soil Organic Carbon Content is an important parameter describing the amount of organic carbon in the soil with the unit [kg/m <sup>2</sup> ]. It always refers to a certain soil depth - f.e. the first metre of the soil, and is integrated over the whole column.
TC	Total Carbon is the amount of carbon in a sample as a fraction in regard to its total weight or volume (unit: [wt% or vol%]). Major sources are organic material from living organisms, carbonates and dissolved CO <sub>2</sub> .
TN	The Total Nitrogen content refers to the amount of Nitrogen in a sample by weight or volume in [wt%] or [vol%].
TOC	Total Organic Carbon is the fraction of all carbon originated from living organisms divided by the total amount of the sample. The unit is either in percentage by weight [wt%] or volume [vol%].
TVC	The Trail Valley Creek camp side is a research facility of the Wilfried Lauries University 50 km north of Inuvik, Canada. In this thesis it is also sampling site.
vol%	Volumetric percentage describes the relative amount of a component by volume.
West	The decimal longitudinal degrees is a unit to describe a position on earth. Together with the latitudinal degrees, each position on the surface can be assigned to one unique combination of Latitudes and Longitudes. Due to the fact that longitudinal degrees are described according to their angle towards prime meridian, they are divided by their position relative to the prime meridian into east and west.
wt%	Gravimetric percentage describes the relative amount of a component by mass.

## Abstract

As a result of strong climatic changes in arctic regions, permafrost areas are subject to substantial modifications. The matter raises global concerns due to the permafrost carbon climate feedback causing large amounts of Greenhouse Gases to be released into the atmosphere. Rising temperatures and climatic changes lead to permafrost disturbances developing distinct features termed thermokarsts.

Thermokarsts evolve when ice-rich permafrost thaws and the soil collapses into the volume previously occupied by ice. In this study, the main focus lies on the thermokarst feature retrogressive thaw slump in the proximity of lakes. The differences in soil parameters between the Active Layer and permafrost and between disturbed and undisturbed permafrost ground are examined to give indications about the parametrical changes of permafrost soils in respect to climate change, permafrost disturbance and the consequent development of thermokarsts. Carbon, nitrogen, grain size, ice content and Radiocarbon dating analysis were conducted for this thesis.

Carbon and Nitrogen are clearly depleted in the active layer compared to values in the cryotic ground and in disturbed compared to undisturbed ground. Further detailed analyses between sites reveal highly fluctuating dynamics and suggest that permafrost disturbance, thermokarst development and hence the release of Greenhouse Gases strongly depends on site-specific features such as vegetation cover, orientation, slope angle, water content and the local landscape history. Although thermokarsts and Greenhouse Gas release are known to increase in the future, how and to what extent controlling factors influence the soils development on a local scale is yet to be determined.

## Zusammenfassung

Infolge der starken Ausprägung globaler Erwärmung in arktischen Regionen sind elementare Veränderung in den Permafrostgebieten zu erwarten. Durch die positive Rückkopplung des Permafrostkohlenstoffs auf den Klimawandel, werden große Mengen von Treibhausgasen in die Atmosphäre freigesetzt. Steigende Temperaturen und veränderte klimatische Bedingungen führen zu Permafroststörungen mit ausgeprägten Landschaftsmerkmalen - genannt Thermokarsts.

Thermokarsts entstehen, wenn eisreicher Permafrost auftaut und der Boden in das zuvor vom Eis eingenommene Volumen kollabiert. In dieser Studie liegt der Fokus auf Thermokarsts mit rückläufigen Hangrutschungen (retrogressive thaw slumps) in der Nähe von Seen. Die Unterschiede in den Bodenparametern zwischen der aktiven Schicht und dem Permafrost, sowie zwischen gestörtem und ungestörtem Permafrostboden werden untersucht, um Hinweise auf die parametrischen Veränderungen der Permafrostböden in Bezug auf Klimaänderung, Permafroststörung und die daraus resultierende Entwicklung von Thermokarsts zu geben. Für diese Arbeit wurden Kohlenstoff-, Stickstoff-, Korngrößen-, Eisgehalts- und Radiokarbon-Datierungsanalysen durchgeführt.

Kohlenstoff und Stickstoff sind in der aktiven Schicht im Vergleich zu Werten im kryotischen Boden deutlich niedriger. Das gleiche gilt auch für Kohlenstoff und Stickstoff in gestörtem im Vergleich zu ungestörtem Boden. Weitere detaillierte Analysen zwischen den Standorten zeigen eine stark schwankende Dynamik und legen nahe, dass Permafroststörung, Thermokarstentwicklung und damit die Freisetzung von Treibhausgasen stark von standortspezifischen Merkmalen wie Vegetationsbedeckung, Orientierung, Hangneigung, Wassergehalt und der lokalen Landschaftsgeschichte abhängt. Obwohl bekannt ist, dass die Thermokarstbildung und die Freisetzung von Treibhausgasen in Zukunft zunehmen werden, ist noch nicht geklärt, wie und in welchem Umfang steuernde Faktoren die Entwicklung der Böden auf lokaler Ebene beeinflussen.

# 1 Introduction

Permafrost areas contain vast amounts of Organic Matter (OM) sequestered over millennia in the soil (Hugelius et al. 2014a,b; Kutzbach et al. 2010; Schuur et al. 2015; Tamocai et al. 2009). As a result of climate change, permafrost areas get disturbed and thermokarst terrain develops and enlarges. When permafrost thaws, previously sequestered Carbon (C) is decomposed by increased microbial activity releasing GHG into the atmosphere (Burn 2011; Everdingen 1998; Grosse et al. 2011; Kokelj and Jorgenson 2013; Kokelj et al. 2009; Marushchak et al. 2011; McGuire et al. 2009; Repo et al. 2009; Romanovsky et al. 2017; Schaefer et al. 2011; Tamocai et al. 2009; Turetsky et al. 2019; Vardy et al. 2000). A changing landscape poses serious threats to settlements in regions with permafrost occurrence and its positive feedback to climate change rises global concerns.

The aim of the thesis is to connect certain soil properties with the degradation of permafrost, in particular at retrogressive thaw slumps. With the aid of several soil parameters, conclusions may be drawn regarding the nature of landscape modifications in arctic regions. The following hypotheses will be investigated:

- I. General properties (ice content, active layer thickness (ALT), bulk densities and radiocarbon dating ( $^{14}\text{C}$ ) measurements) are expected to reflect typical characteristics of permafrost soils in the Northwestern Territories (NWT), Canada (Burn and Michel 1988; Kokelj and Burn 2003, 2005; Kokelj et al. 2002; Lacelle et al. 2004; Mackay 1983; Ping et al. 2008; Tarnocai and Bockheim 2011).
- II. Biochemical compounds (Total Organic Carbon (TOC), Total Carbon (TC) and Total Nitrogen (TN)) are expected to be depleted in the active layer (AL) indicating higher (mineralisation) rates compared to the cryotic ground (Broll et al. 1999; Pries et al. 2012; Schuur et al. 2015; Sollins et al. 1984; Stevenson 1994; Strauss 2010; Vardy et al. 2000; Walthert et al. 2004). The grain size distribution (GSD) may show translocation dynamics in finer grain fractions (Broll et al. 1999; Kokelj and Burn 2003; Locke 1986; Tarnocai and Bockheim 2011)
- III. Comparison between disturbed and undisturbed categorised sites is consulted to reveal processes within soil profiles connected to thermokarst development, thawing of permafrost and deepening ALT. At disturbed sites, increasing temperatures may result in deeper ALT with increasing mineralisation rates exhibiting lower C and TN contents and narrower Total Organic Carbon to Total Nitrogen ratio (C/N ratio) (Brouchkov

et al. 2004; Burn 1997; Lacelle et al. 2010; Lantz et al. 2009; Nixon and Taylor 1998; Strauss 2010; Vardy et al. 1998).

## 1.1 Scientific background

### 1.1.1 Permafrost distribution and properties

Permafrost is defined as ground material containing ice and organic materials which exhibits a temperature regime lower than 0 °C for at least two consecutive years (Brown and Kupsch 1974; Everdingen 1998). The development of terrestrial permafrost (exclusively referred to in this thesis) is mainly controlled by prevailing climatic conditions but also by the historic landscape evolution and the altitude of the landscape. That is why permafrost can occur around the globe to differing extents.

Globally, 16–21 \* 10<sup>6</sup> square kilometres (km<sup>2</sup>) of the exposed land surface is estimated to exhibit permafrost conditions (Gruber 2012). This accounts for 12.4–16.3 % of the exposed land surface. Permafrost occurs in higher quantities on the northern hemisphere (13–18\*10<sup>6</sup> km<sup>2</sup> north of 60 degrees South) due to its larger land surface area (Gruber 2012). Its thickness can range from a few metres up to 1.5 kilometres (km) (Black 1954; Kitover et al. 2016; Kutzbach et al. 2010).

The permafrost temperature changes with depth and develops a general vertical structure controlled by thermal fluxes between the cryotic ground and the layers below and above (Figure A1, Appendix). The depth of the permafrost base is only influenced by the geothermal fluxes from the core of the planet and its formation history. The depth where seasonal temperature fluctuations almost cease to persist (temperature change <0.1 °C), is termed Depth of Zero Annual Amplitude (DZAA) (Everdingen 1998). The layers above the DZAA experiences heat loss in winter, hence get colder, while it is supplied with thermal energy in summer. On the annual average, the temperatures decrease from bottom to top. The highest temperature fluctuations of the cryotic ground happen at the permafrost table due to seasonal influences.

The upper boundary of the permafrost is called frost/permafrost table or thawing front and usually coincides with the 0 °C isotherm which fluctuates seasonally and annually (Everdingen 1998). Above the permafrost lies the AL. It is characterised by annual thawing and freezing in summer and winter respectively. Areas of constantly non-cryotic ground due to thermal anomalies are called taliks and are strongly influenced by lake and river dynamics as well as salinity, pressure and water content.

The temperature of the cryotic ground is the key parameter for determining

the state of the permafrost. It is measured at the DZAA, and is used to identify long-term trends. The temperature ranges from 0 to  $-23.6$  °C on the southern hemisphere and from 0 to  $-15$  °C on the northern hemisphere (IPCC 2013; Romanovsky et al. 2010a). Generally the lowest temperatures are observed in permafrost areas closest to the poles and they increase towards the equator, although there are substantial differences on the same latitudes owing to varying climatic and geothermal influences. Ice content, exposition, slope, vegetation and snow cover and thermal soil and rock properties also constitute the features of the permafrost on a local scale. Thermal properties are mainly controlled by soil moisture and minimum winter temperatures (Schuh et al. 2017).

Changes in permafrost temperatures, in particular in the first few metres of the soil, imply severe alteration of the soil functioning as a C sink and have therefore consequences for the global climate.

### 1.1.2 Permafrost carbon climate feedback

Observations show that the polar regions (60-90 degrees North) experience a substantially stronger change in surface air temperature of up to  $0.755 \pm 0.106$  °C per decade between 1998-2012 as compared to global average change of up to  $0.112 \pm 0.008$  °C per decade in the same time period (Huang et al. 2017). Changes in surface air temperatures have strong implications for the state of permafrost.

The ground temperature near the DZAA of 123 boreholes exhibit a global mean temperature increase by  $0.29 \pm 0.12$  °C between 2007 and 2016 and by 2 - 4 °C in the circumpolar Arctic since the 1970s (Biskaborn et al. 2019). Data also show an increase of ALT in the northern hemisphere in a 22-years data set, yet the high spatial variability and strong inter-annual fluctuations hinder predictions (Hinkel and Nelson 2003; Shiklomanov et al. 2016). Investigating future permafrost dynamics are important to understand due to its implications on biochemical fluxes between the atmosphere and the soil. Water saturation, little access to oxygen and low temperatures minimise the microbial degradation of organic matter significantly which allows the soil to accumulate large quantities of C from remnants of plants and animals in terrestrial soils and sediments over huge time periods.

There exists a wide range of estimates concerning the amount of C stored within permafrost soils and sediments. These estimates are highly uncertain and vary greatly, though many scientists agree that it is more C than stored in the global vegetation and more than twice the amount already in the atmosphere (Hugelius et al. 2014a; Kutzbach et al. 2010; Schuur et al. 2015;

Tamocai et al. 2009). The sequestered C relevant for current climatic concerns resides in the first few metres of soils. According to Hugelius et al. 2014b the circumpolar C storage in the first 3 metres of the soil amount  $1300 \pm 200$  pentagramm (Pg), most of it (ca. 800 Pg) stored in permafrost terrain. When these soil layers with sequestered C reach favourable conditions for mineralisation, such as warmer temperatures and access to oxygen, microbes extract energy by breaking down the organic matter and release GHG into the atmosphere (mainly carbon dioxide ( $\text{CO}_2$ ), methane ( $\text{CH}_4$ ) and nitrous oxide ( $\text{N}_2\text{O}$ )) (Marushchak et al. 2011; Repo et al. 2009; Schaefer et al. 2011; Tamocai et al. 2009; Vardy et al. 2000). There, the GHG are radiatively active and store thermal radiation increasing global temperatures. A warming climate alters the C cycle and the permafrost areas turn from a C sink into a source for the atmosphere (Figure 1) causing a positive feedback to global warming - called permafrost carbon climate feedback (Strauss et al. 2017).

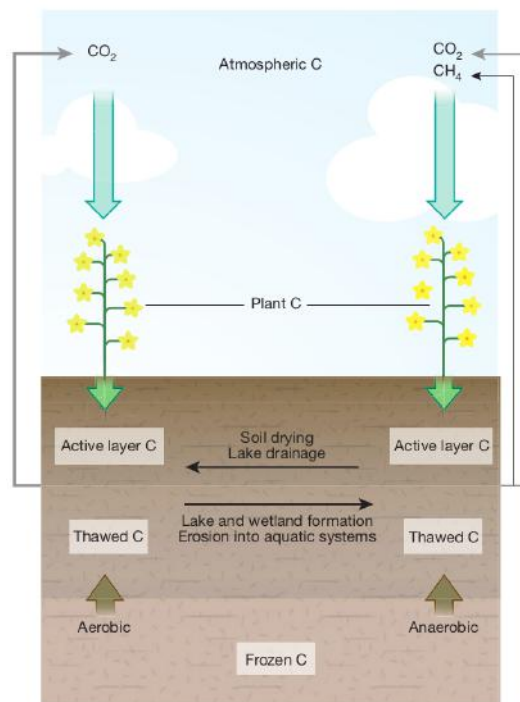


Figure 1: Permafrost Cycle (Schuur et al. 2015). When the temperatures rise, the ALT increases and C is released into the atmosphere.

For estimating C release, the soil composition as well as the hydrological regime are equally important. In anaerobic environments, C is released to a greater extent as  $\text{CH}_4$ , which has a 21 times higher potential impact on climate over a 100-years scale compared to  $\text{CO}_2$  (IPCC 2013) whereas in aerobic environments the total loss of C is greater and has a higher impact on climate (Schuur et al. 2015). Depending on the amount of C in soil, the release of GHG differs significantly. Mineral ( $< 20\%$  C) and organic ( $> 20\%$  C) soils feature decade losses of 6-13% and 17-34% respectively (Schuur et al. 2015).

The magnitude of C release from permafrost soils is strongly linked to the C/N ratio (Table 1). Microbes breaking down C for energy, use nutrients such as nitrogen (N), which remain in the vegetation or the soil whereas C is released as GHG. Consequently, a wide C/N ratio indicates a low rate of mineralisation and hence the potential for further decomposing of C (Sollins et al. 1984; Stevenson 1994; Strauss 2010; Walthert et al. 2004).

Under the current climate warming trajectory Representative Concentration

*Table 1: Classification of mineralisation rate according to C/N ratio in soils after Walthert et al. 2004*

<b>TOC/TN- ratio</b>	<b>Description</b>	<b>Rate of mineralisation</b>
<10	very narrow	high
10-12	narrow	
13-16	moderately narrow	moderate
17-20	moderate	
21-25	moderately wide	
26-35	wide	low
>35	very wide	

Pathway (RCP) 8.5, model scenarios suggest a potential C release from permafrost zones to be in the range of 37-174 Pg C with an average of 92 Pg C across models by 2100 (Schuur et al. 2015). This translates into a contributing warming potential of up to 0.27 °C by 2100.

As permafrost degrades, the thickness and areal extent decrease, the ALT deepens, taliks and lakes can develop and enlarge, and the landscape changes geomorphologically and GHG release is increased (Burn 2011; Everdingen 1998; Kokelj and Jorgenson 2013; Kokelj et al. 2009; Romanovsky et al. 2017).

Strauss et al. (2017) mentions four different explanations why permafrost degrades: (I) An increased unfrozen water content and ground warming, (II) deepening of the ALT, (III) thermo-erosion along lakes, rivers and coasts and (IV) rapid thaw due to thermokarst and thermo-erosional processes. Morgenstern (2012) points out that the two main reasons for permafrost degradation are thermokarsts and thermo-erosional processes which strongly modify the landscape and enhance permafrost degradation on a local scale. Understanding their dynamics regarding GHG release and landscape evolution is therefore highly important.

### **1.1.3 Thermokarst**

Thermokarst terrain develops when ground ice melts or permafrost thaws and the soil collapses into the volume previously occupied by ice (Everdingen

1998). The process itself is termed thermokarst leading to typical thermokarst terrain and landforms. It enhances the permafrost degradation and microbial activity by lowering the water table and exposing previously cryotic ground (Kokelj and Jorgenson 2013; Romanovsky et al. 2017). Landforms with thermokarst features are mainly constrained to ice-rich glaciogenic deposits and are mostly absent from non-glaciated terrain and Holocene alluviums (Kokelj et al. 2017). Preferentially, they evolve in environments with at least a slight slope gradient and excess of water and ice, causing large volumes of thawed material to be transported into fluvial, coastal and lacustrine environments (Chin et al. 2016; Kokelj et al. 2005; Lantz et al. 2009; Shur and Jorgenson 2007).

Under varying conditions the thermal equilibrium can be disrupted by geomorphic, vegetational or climatic processes, either natural or man-induced. Warmer air temperatures, increased rainfall and changes in snow and vegetation cover have been identified as main drivers of permafrost degradation (Biskaborn et al. 2019; Burn and Kokelj 2009; Kokelj and Jorgenson 2013; Osterkamp 2007a,b; Romanovsky et al. 2010a,b; Shur and Jorgenson 2007; Zhang and Stamnes 1998). These changes can cause a thermal disturbance of up to 6 °C compared to undisturbed ground (Burn 2011). Initiating events such as extreme thaw or high precipitation can result in thaw subsidence of permafrost causing the degradation of permafrost (Lacelle et al. 2010; Lantz et al. 2009).

Thermokarst development is generally expected to accelerate and intensify with warming temperatures, since more permafrost is affected by thawing (Kokelj and Jorgenson 2013; Murton 2009). Increasing thermokarst activity indicates a rejuvenation of post-glacial landscape by mobilising previously cryotic glaciogenic deposits transforming large parts of the landscape.

Thermokarsts and their impact are complex and consist of positive and negative feedbacks. Several thermokarst landforms are associated with processes of permafrost degradation. One of the largest and most impacting thermokarst features on a local scale are retrogressive thaw slumps.

Retrogressive thaw slumps are big geomorphic features which can impact an area of tens of hectares and can displace volumes of a magnitude of  $10^6$  m<sup>3</sup> of thawed material (Lantuit and Pollard 2008). Determining probable initiating events is problematic since large slumps take years to evolve and may exhibit a polycyclic nature referring to a development of new thaw slumps within the slump floor of older retrogressive failures (Kokelj and Jorgenson 2013). They occur along streams, rivers and coasts (mechanical erosion), at lakes (thermally driven) and at slopes (extreme thaw and precipitation events) comprising a distinct structure (Figure 2).

Ice-rich ground is exposed and ablated through retrogressive failure of the

soil at the headwall. Depending on the magnitude of the retrogressive failure, headwalls can be up to tens of metres high. Headwalls of thaw slumps at coasts can continue to retreat at rates of 10 metre per year (m/a) for decades and reach a peak headwall retreat of up to 30 metre (m) in exceptional years (Lantuit and Pollard 2005). At the slump floor debris accumulates and is transported downslope by rainfall-induced, fluvial and gravitational processes. At the foot of a slump, where the slope flattens out, when no stream or river is erosively active, an alluvial fan-shaped lobe of debris can form.

Stabilisation of thaw slumps occur when sufficient material accumulates in

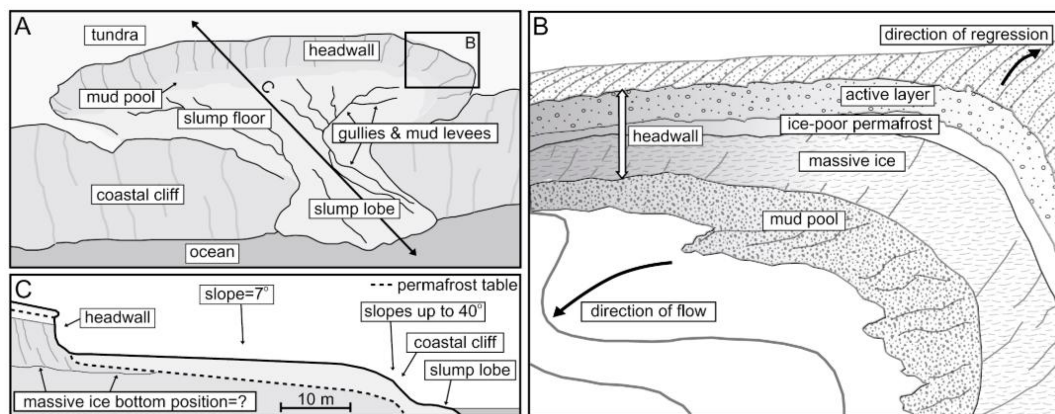


Figure 2: Schematic of retrogressive thaw slumps (A), headwall (B) and (C) cross-section structures after Lantuit and Pollard 2005

front of the headwall and vegetation starts to cover the slump area and impede further thawing of ground ice. It may be several decades before thaw slumps are stabilised (Burn 2011).

Generally, larger slumps retreat more rapidly due to positive feedbacks such as larger exposition to solar radiation, higher rate of ablation and more efficient debris transport. Kokelj et al. 2017 shows that the erosion intensity, the relative relief and therefore also the disturbance density is the highest at fluvial and coastal environments. Thaw slump activity has accelerated with climate change and is expected to increase in the future, in particular due to increases in rainfall (Gooseff et al. 2009; Kokelj et al. 2015b; Lantuit and Pollard 2008; Lantz and Kokelj 2008).

Thermokarst development has gained scientific interest due to its implication on the C cycle (Grosse et al. 2011; Turetsky et al. 2019). Roughly 20 % of the northern permafrost area is covered by thermokarst landforms and the unstable areas are also expected to be the most carbon-rich (Olefeldt et al. 2016). In recent literature the term “abrupt thawing” has evolved referring to fast developing thermokarst features which have a similar climate impact as gradual thawing thermokarst due to their greater release of methane (Koven et al. 2015; Turetsky et al. 2019). The presence of abrupt thawing is expected

to amplify C release by 50 % although effecting less than 20 % of the landscape (Turetsky et al. 2019).

To determine overall changes in permafrost regions, the analysis of specific soil parameters are necessary to reveal small processes within the soil effecting the landscape on a larger scale.

#### 1.1.4 Soil Properties

In arctic regions, soil genesis is dominated by cryogenic processes due to its cold climatic conditions (Margesin 2009). Stresses and pressures created by expanding ice and contracting soil material due to temperature changes, translocate, rearrange and deform materials and solutes leading to unique soil characteristic in permafrost-affected soils. Dominantly, the presence and movement of unfrozen soil water towards the permafrost table drives these cryogenic processes such as freeze-thaw, frost heave, cryoturbation, thermal cracking, cryogenic sorting, cryodesiccation, gleying, eluviation, brunification and salinization (Bockheim 2007; Ping et al. 2008; Vandenberghe 2013). Although most of these processes occur in the AL, they also affect the near-surface permafrost due to fluctuations in permafrost table depth (Ping et al. 1998). The subsurface soil horizons commonly exhibit a blocky, platy structure and are associated with higher bulk densities. Typical features are irregular and broken soil horizons, organic intrusions and accumulation, silt-enriched layers and caps, granular structures and vein formations disrupting the general horizontal organisations of the soil (Figure 3) (Ping et al. 2008; Tarnocai and Bockheim 2011; Tarnocai and Smith 1992; Vandenberghe 2013; Vardy et al. 2000). These characteristics define the movement of water through and the thermal properties of the soil dictating its past and prospective evolution.

When water percolates along the thermal gradient from warm to cold, it refreezes in the subsoil increasing the ice thickness and volume over time at the permafrost table. The occurrence of large ice volumes in permafrost has strong implications on the stability of soil (Chapter 1.1.3). This pattern is visible in moisture and soluble content profiles and fine organic and inorganic matter accumulation layers enriching the lower AL and near-surface permafrost in mineral and organic soils (Kokelj and Burn 2005; Kokelj et al. 2002; Tarnocai 1972; Wang et al. 2009). Relict active layer thicknesses can be determined by finding these accumulation layers (Kokelj et al. 2002).

In general, deeper layers have older organic material than upper layers due to the order of sedimentation and accumulation of organic C. Root penetration and soil reworking processes lead to mixed layers with differing ages. With aid of the  $^{14}\text{C}$  method, the age of each layer and the accumulation periods can be

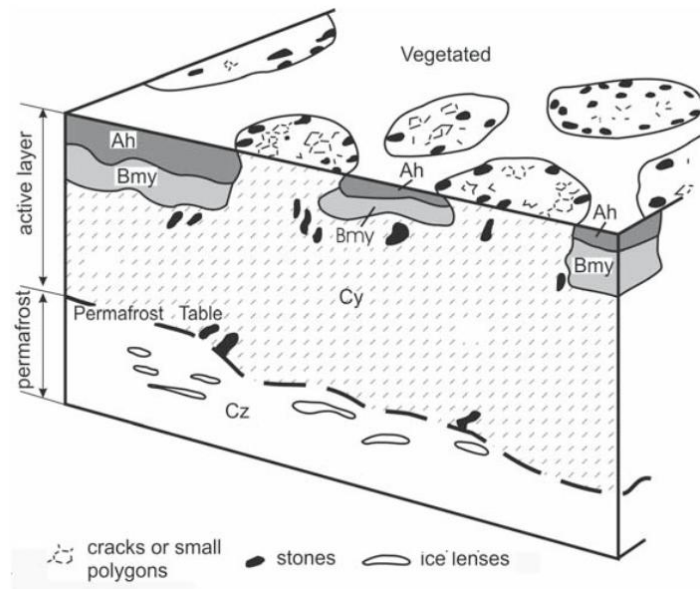


Figure 3: Schematic showing a non-sorted soil profile with broken cryoturbated soil horizons (y), strongly indurated B-horizons (m), accumulated organic matter at surface (h) and accumulated solubles in the C-horizon (z) (Margesin 2009)

determined.

After the retreat of the glaciers, thermokarst activities and cryogenic processes reworked the soil and mixed the layers which may have led to younger OM in deeper layers (Akerman 2005; Lacelle et al. 2004; Pries et al. 2012). In particular, in the first metre of the soil the mixing of layers has been observed (Pries et al. 2012).

Cryoturbated soils in the arctic tundra of Canada contain substantially higher Soil Organic Carbon Content (SOCC) values compared to soils without cryoturbation (49 to 61 kilograms per square metre ( $\text{kg}/\text{m}^2$ ) compared to 12 to 17  $\text{kg}/\text{m}^2$  respectively) (Tarnocai and Bockheim 2011). According to King et al. (2008) organic soils consist of much higher organic content (43 to 144  $\text{kg}/\text{m}^2$ ) than mineral soils (49 to 61  $\text{kg}/\text{m}^2$ ). The rates of organic accumulation are controlled by different environmental factors such as orientation, slope angle or nutrition availability (Chapin et al. 2002; Pries et al. 2012; Shaver et al. 1992).

In contrast to these vast organic accumulations in the AL and the permafrost, N contents are generally very low ( $< 1$  gravimetric percentage (wt%) or  $< 10$  g/kg TN) limiting plant growth and are mainly stored in the surface organic matter and the vegetation and decline with increasing depth (Broll et al. 1999). N can only be taken up by living plants where roots can penetrate the soil and the uptake of N is therefore restricted to the AL. Other processes of N depletion is through microbial activity releasing the GHG  $\text{N}_2\text{O}$  into the atmosphere (Chapter 1.1.2).

The C/N ratio is narrow in the AL indicating the rate of mineralisation (see Chapter 1.1.2, Sollins et al. 1984; Stevenson 1994; Strauss 2010; Walthert et al. 2004). It is wider in the permafrost where perennially cryotic ground prohibits mineralisation and similarly wide in the lower layers of the AL due to anaerobic conditions (Weintraub and Schimel 2005) releasing GHG at a much slower rate (Gundelwein et al. 2007; Hinkel et al. 2001; Lacelle et al. 2010; Schuur et al. 2015; Tarnocai and Bockheim 2011; Vardy et al. 2000; Wang et al. 2009). High organic material leads to lower bulk densities which increase with depth when the OM diminish and the soil texture changes to having more consolidated material (Vardy et al. 2000).

Studies mention dynamics where sediments are mobilised leading to a depletion of finer sediments in upper layers, a process occurring since the Holocene warming period to varying extents (Lacelle et al. 2004; Locke 1986). As silt is more prone to translocation developing silt-enriched layers and silt caps in the AL and as water mobilises finer sediments (clay and silt), a grain size differentiation can be observed (Bockheim and Tarnocai 1998; Lacelle et al. 2004; Locke 1986; Tarnocai and Bockheim 2011).

This study examines the changes in soil parameters between disturbed and undisturbed ground mainly at retrogressive thaw slumps. Disturbance categories are therefore introduced for comparison.

## 1.2 Site description

The study area is located north of Inuvik, Northwest Territories, Canada, south-east of the Mackenzie River Delta (Figure 4). It lies in the Mackenzie region where elevations vary between 9 and 187 m above sea level. The terrain with gently rolling hills and some deep river valleys has a mean slope angle of 3 ° (Marsh et al. 2010).

The underlying bedrock is primarily Cretaceous and Tertiary clastic and sedimentary rock (Dixon et al. 1992; Rampton 1988). The arctic coastal plain north of Inuvik is characterised by Pleistocene coarse grained fluvial, deltaic and estuarine sediments overlain by extensive sheets of ice-containing sediments with interbedded peat layers covered with morainal deposits and a thin organic layer on top (Mackay 1963). According to Rampton 1988 the study area is subdivided into the Anderson Plain with the South Caribou Hills and the Tuktoyaktuk Coastal Plain with the Eskimo Lakes Pitted Plain (Figure 4).

All sampling locations apart from Lake 6 lie within the elevated Caribou Hills (Rampton 1988). Sample site Lake 1 lies in the centre of the plain whereas Lake 11, 12, Trail Valley Creek (TVC) and 1sub3 at the boarder to the Eskimo

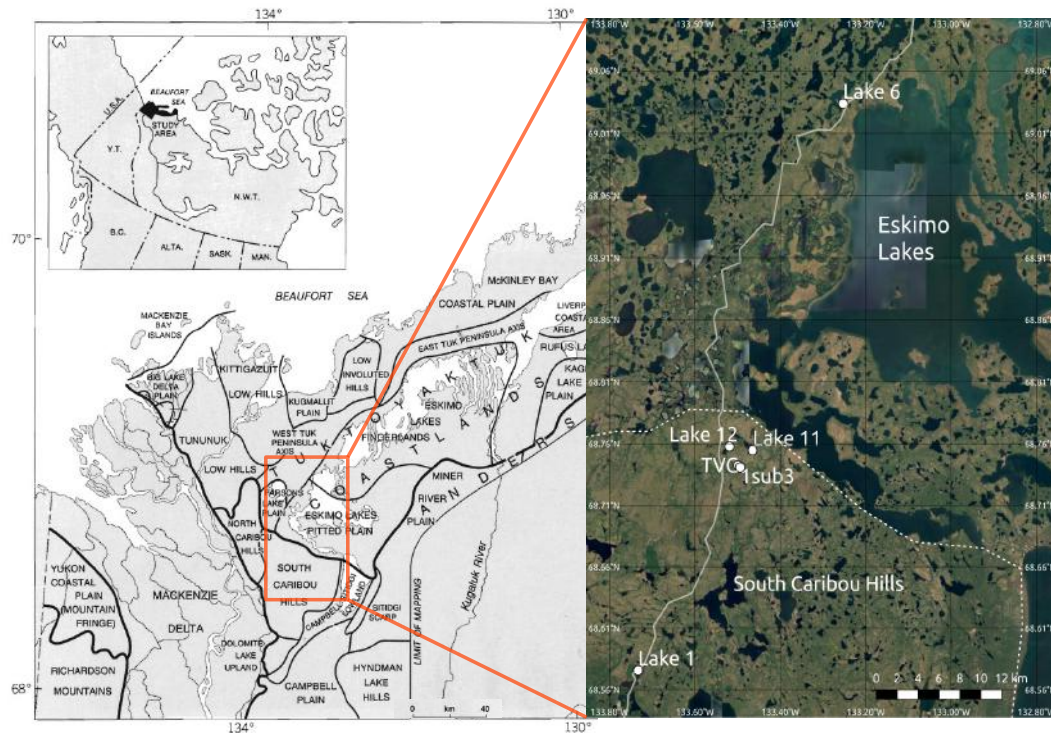


Figure 4: Physiographic subdivision of Tuktoyaktuk Coastlands and adjacent areas of the Geological Survey Canada (Rampton 1988) (left). The study area lies within the South Caribou Hills and the Eskimo Lakes Pitted Plain. Eskimo Lakes are north of most study sites apart from Lake 6 which lies west of them. Overview map of study sites (right). White line indicates the Tuktoyaktuk-Inuvik-Highway. Dashed line indicates the north-eastern boundaries of the South Caribou Hills modified from Rampton 1988. Background map is created with an satellite imagery map from 2017 provided by Google (Google Maps 2017).

Lakes Pitted Plain. The site Lake 6 is located at the Eskimo Lakes further north. More detailed maps are displayed in the appendix from Figure A2 to A11.

The Caribou Hills is a bedrock controlled landform and is well elevated above the surrounding area. The surficial geology of the study area is dominated by morainal deposits developed during the Toker Point Stade of the Early Wisconsinan glaciation (Pleistocene). It consist also of glaciofluvial out-washes from plain and valley trains around the Eskimo Lake (Late Wisconsinan glaciation, Sitidgi Stade), lacustrine deposits around relict or still existing lakes (< 15% lake cover (Mackay 1963)) and colluvial deposits formed later in the Holocene (Rampton 1987).

At the outer perimeter, the area is characterised by sharp escarpments in the east and north but more gentle in the south leading to a radial drainage system with broad melt-water channels. Except from small depressions, the Caribou Hills are well drained with thin unconsolidated, coarse-grained material which often is more than 13 m thick (Rampton 1988). There are well-laminated and

cross-bedded silts, sands and gravels inter-stratified with up to 90 centimetres (cm) thick peat beds. They indicate a previous position of the Mackenzie Delta due to post-glacial changes in sea level and a possible different course of the Mackenzie River into the Liverpool Bay (north-east of study site in Figure 4) with climatic conditions probably similar to the present (Mackay 1963). The landscape at the Caribou Hills was highly modified by thaw processes in the past which abated and permafrost could accumulate again (Kokelj et al. 2002).

According to Dyke and Prest 1987 large parts of the Mackenzie Delta and its margins were deglaciated ca. 12-13  $10^3$  years (ka) ago but organic material did not begin to accumulate before 8 ka ago - at least in this study area (Clark et al. 2009; Dyke and Evans 2014; Kitover et al. 2016).

The current climate is characterised by long cold winters and short summers, with a snow cover period of 8 months. The mean annual temperature is  $-10$  °C and the mean annual precipitation is roughly 260 mm whereof 60 % falls as snow (Marsh et al. 2010). Rampton 1988 determined an annual near-surface ground temperature between  $-5$  and  $-6$  °C in the Caribou Hills but recent data mentioned temperatures up to  $-1.7$  °C (Grünberg et al. 2020). The study area is underlain by ice-rich continuous permafrost at the edge of the forest-tundra transition zone. Extensive sheets of ice are common with an AL ranging from 0.3 to 0.8 m at sites without apparent permafrost degradation (Marsh et al. 2010).

Compared to other regions in Northwest Territories (e.g. The Peel Plateau), the study area features a low density of thaw slumps due to gentle topographic gradients and abated thawing after the early Holocene warming period (Murton 2001). It is known to have experienced strong modification by thermokarst processes in the past shaping today's landscape (Rampton 1988).

### 1.3 Disturbance categories

Disturbance categories are implemented to connect permafrost degradation with certain soil processes. Based on experience and visual classification of the sites, disturbed-categorised ground (in plots and table referred to as "yes") is expected to develop a distinct pattern compared to non-disturbed ground ("no").

Each sample location was categorised according to its aforementioned level of degradation. For assigning each sample location to its category, maps, the field book notes and pictures are advised. Aerial pictures and satellite images are commonly utilised for visual classification and identification (Kokelj et al. 2015a,b; Lacelle et al. 2015; Lantz and Kokelj 2008).

Inside the head wall the ground is categorised as disturbed, often indicated by bare soil at the surface (sign of soil erosion) with no vegetation on top (Figure 5a). Samples taken at the headwall and the close proximity of it, are also categorised as disturbed since it is the position of ablation where thaw slumps advance and enlarge (Figure 5b).

The vegetation cover is also taken into account when categorising the sites (Burn 2011; Burn and Friele 1989). High and dense vegetation has proven to be an indicator for disturbance but is no prerequisite for disturbed ground (Figure 6). At water bodies and small channels with apparent flowing or standing water a disturbance is also expected due to the thermal influence of the water (see Chapter 1.1.3) (Kokelj and Jorgenson 2013).

Areas not effected by disturbances are identified by no obvious presence of soil erosion or mass movement indicated by the typical short vegetation cover (Figure 7). The absence of standing or flowing water is also important when categorising sites as undisturbed.



(a) Bare soil inside the thaw slump at Lake 6 indicates typical slope failure and mass movements. In the far back of the picture the headwall stands out. (Picture taken from inside the thaw slump at Lake 6 on 20th of August, 2018 by Julia Boike, Alfred-Wegener Institut, Helmholtz-Zentrum für Polar- und Meeresforschung (AWI))



(b) A strongly exposed, vertical headwall section at Lake 6 (Picture take on 20th of August, 2018 by Bill Cable, AWI).

Figure 5: Examples of sites categorised as disturbed at Lake 6 [69.0066 Northern decimal latitudinal degrees (North), 133.3634 Western decimal longitudinal degrees (West)].



(a) Picture taken from headwall downwards towards the lake. Thaw slump is in the centre of the picture.



(b) Picture taken upwards towards the head wall from inside of the thaw slump visible in Figure (a).

Figure 6: High vegetation with willow shrubs (a) and high grass cover (b) in and around the thaw slump are typical for highly disturbed areas. Location at Lake 6 [69.0066 North, 133.3634 West] (Pictures taken on 20th of August, 2018 by Inge Grünberg, AWI).



Figure 7: Typical site defined as undisturbed without any sign of soil erosion or depressions. Typical vegetation cover are lichens, tussock sedges, tundra moss and dwarf shrubs [69.0066 North, -133.3634 West] (Pictures taken by Inge Grünberg, AWI).

## 2 Methods

### 2.1 Sample extraction in-situ

The data was obtained during the MOSES expedition<sup>1</sup> to the Northwest Territory of Canada in August 2018. Permafrost and/or AL samples were taken at six different locations along the Inuvik-Tuktoyaktuk-Highway. The locations Lake 1, TVC and 1sub3 were sampled at undisturbed sites (Figure A2 and A5). At Lake 6, 11 and 12 several sample points were set along a

<sup>1</sup>[https://www.ufz.de/export/data/470/236390\\_mCAN2018\\_Report.pdf](https://www.ufz.de/export/data/470/236390_mCAN2018_Report.pdf) (Accessed on 25th June 2020)

transect from undisturbed tundra through retrogressive thaw slumps to lake shores (Figure A3, A4 and A6). At Lake 1, TVC and 1sub3 a pit was dug through the AL down to the frost table boundary for permafrost core extraction (Figure 8). The battery powered mini-SIPRE Coring Auger (Figure 9) drills



*Figure 8: Lake 1, first pit after drilling the first core. (Picture take on 17th August, 2018 by Julia Boike, AWI)*

down to almost one metre with a coring barrel extracting a core of 5 cm in diameter. Depending on the composition of the ground (e. g. stones inhibit the drilling), the auger extracted cores of 7-60 cm in length.

The parts were subsequently packed in plastic bags (Figure 10). During this step, care had to be taken to label the depths of each core section accurately and indicate the top and the bottom of the core.

Frozen samples were put within hours of sampling into a freezer and all samples were transported in a cooling container with ice packs back to Germany. The ice packs were successful in keeping the samples frozen during the journey, as shown by the temperature data collected by a logger in the cooler.

The AL soil samples were taken at different depths in the same pits where frozen core samples were drilled. The samples were simply filled into Falcon tubes or into plastic bags. Additionally, at each site the ALT and the vegetation types were noted.

At sites where no pit was dug, AL soil samples were extracted with a 2 cm in diameter soil sampling probe<sup>2</sup> extracting samples from a maximum depth of 1 m.

The extended data set with ALT measurements of Inge Grünberg, AWI exhibits a different sampling setup than the main data set. Although the areas remain the same (e.g. Lake 1, 6...etc.), there are more sampling positions in each area than obtained for the main data set. Detailed maps are shown in

---

<sup>2</sup><https://www.ams-samplers.com/7-8-x-33-sst-soil-probe-w-handle.html> [Accessed on 26th June, 2020]



(a)



(b)

Figure 9: (a) Testing of the battery powered mini-SIPRE Coring Auger at Lake 1 - Position 1 [68.575479 North, 133.73358 West] (Picture taken on 17th of August, 2018 by Julia Boike, AWI); (b) One metre coring barrel extracting a 5 cm in diameter core (Picture taken by Frieder Tautz)

the appendix (Figure A7 to A11).

## 2.2 Active layer and permafrost subsampling

The cores were taken out of the freezing room ( $-25^{\circ}\text{C}$ ) and aligned along the folding rule on aluminium foil in the cooling chamber ( $-4^{\circ}\text{C}$ ) giving an overview over each core (Figure 12). Not every subsection (individual pieces of the core) was sampled for every parameter. It was decided for each core section individually what subsamples are to be taken. Leftovers, referred to as “Extra” were saved for further or repeated analyses (Figure 13).

Ideally, the subsamples were extracted from the centre of the core since the outside of the core was not representative caused by thawing and refreezing during transportation. Evidently thawed parts or pieces of the core which could not be assigned properly to the core sequence, were cut off and discarded.

The weight of the sub-samples was acquired, together with the Nasco Whirl-Packs plastic bags, so that the actual weight of the sample could be calculated by subtracting the average weight of one bag. The tools for dissecting the subsections were a knife and Makita band-saw.

Firstly, each core was sampled at least once for 14C. A few grams were put



Figure 10: Aligning the core after drilling (a) and packing it in plastic bags (b) at Lake 6, Pit [69.033713 North, 133.253694 West] (Picture taken on 20th of August, 2018 by Julia Boike, AWI)



Figure 11: AL soil samples taken at study site Lake 11 on 24th August, 2018 (Pictures on 6th and 7th November, 2018 taken by Frieder Tautz)

into an annealed jar with aluminium foil underneath the lid. These samples were analysed in the AWI laboratories MICADAS in Bremerhaven.

Secondly, suitably sized subsections were cut with the band-saw into cuboids or cylinders and determined for their volume and their weight. These samples were used to analyse the ice content and the according bulk densities in the AWI laboratories in Potsdam.

Thirdly, small pieces were put into plastic cans for the analysis of TOC, TC, TN and grain size in the AWI laboratories in Potsdam.

Further subsamples were taken from soil samples extracted from above the frost table boundary. They have been kept frozen after being taken from the soil and subsampled for TOC, TC, TN, grain size and 14C. The 14C subsamples were only taken once per soil profile.

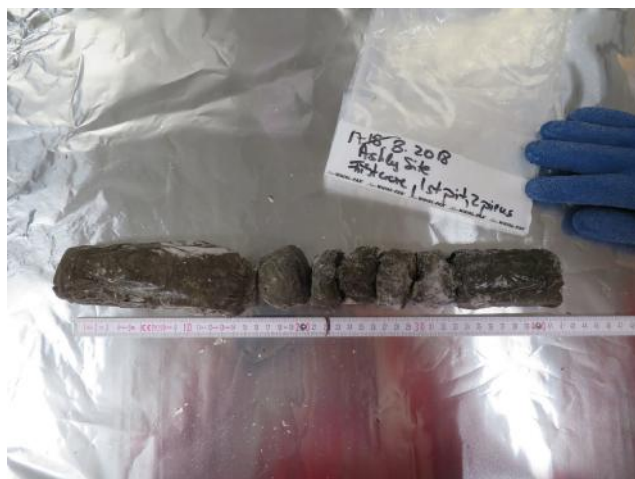


Figure 12: First core taken at Lake 1 at the first pit aligned on aluminium foil in cooling chamber at  $-4^{\circ}\text{C}$  (Picture taken on 15th of November, 2018 by Frieder Tautz)

## 2.3 Laboratory Analyses

The following analyses were conducted for this thesis' objectives. All measurements done in the laboratories at AWI, Potsdam were obtained by the author. The other measurements were send to the appropriate laboratories of AWI.

- Biochemistry: TC, TN, TOC (AWI Potsdam)
- Grain size analysis (AWI Potsdam)
- Ice content (AWI Potsdam)
- Radiocarbon dating ( $^{14}\text{C}$ ) (AWI, Bremerhaven)

### 2.3.1 Biochemistry

The quantitative analysis of TC, TN and TOC of the samples were determined with the gas-phase chromatograph (Elementar Analysensystem GmbH Vario MAX-C for TOC; Elementar Analysensystem GmbH Vario EL III for TC and TN). The main principle of gas-phase chromatography is based on catalytic tube combustion with oxygen supply at high temperatures to incinerate the compounds of the sample and change the aggregate state to gaseous. With an unreactive carrier gas (mobile phase), the gaseous sample is then transported through a tube/column with a specific filling (stationary phase) interacting with the gas. Each compound takes different times to pass through and exit the column due to different chemical and physical properties (retention time). Since the compounds are separated from each other and the elements are detected and identified electronically, it is possible to analyse each element qualitatively and quantitatively.



Figure 13: Subsampling for different analyses in cooling chamber: Nasco Whirl-Pack referred to as “Extra” as backup samples for subsequent analyses if necessary and the cuboid for ice content. The plastic tins are for TOC, TN, TC and GSD. The 1.5 millilitre (ml) Safe-Lock Tube for microbial sequencing (data not included in this thesis). The glass jar for  $^{14}\text{C}$  analysis. (Picture taken on 6th of November, 2018 by Frieder Tautz)

The subsamples for the biochemical analysis (TOC, TC, TN) were freeze-dried (Sublimator 2-4-5, Zirbus Technology) and subsequently milled in agate grinding jars (Planetary mill Pulverisette 5, Fritsch). Of the ground material  $8 \pm 0.005$  milligram (mg) was filled into 50 mg tin boats together with tungsten oxide for assuring complete incineration of the sample. These small containers needed to be folded in such a way that no material is being lost during the process, because the exact weight of the sample is crucial for the analysis. The TOC samples were put and weight into crucibles instead of tin boats. The amount was dependent on the TC values obtained beforehand. Additionally, the gas-phase chromatograph required standard samples every 15 measurements with known amounts of the measured compounds to ensure correct analytical values, which were also filled into the tin boats or crucibles respectively. To eliminate possible errors each sample is measured twice.

### 2.3.2 Grain size analysis

This analysis is based on the diffraction of light by particles passing through a laser beam. The intensity of the light scattered by a particle is directly proportional to the particle size and indirectly proportional to the angle of the laser beam (Fraunhofer diffraction).

The organic compounds of the sample needed to be removed with Hydrogen peroxide ( $\text{H}_2\text{O}_2$ ) to measure only clastic grains. For at least two weeks, 10 ml of 30% acetic acid ( $\text{CH}_3\text{COOH}$ ) was added daily to the dried sample mixed with a 3 %  $\text{H}_2\text{O}_2$  solution.

The pH had to be controlled by adding Ammoniac or  $\text{CH}_3\text{COOH}$  accordingly to ensure the pH to be within the range of 6.5-8. The samples were put on a heating shaker at  $60^\circ\text{C}$  to enhance the reaction and inhibit conglomeration at the bottom of the beaker glasses (Edmund Bühler GmbH SM 30 AT control). When the reaction of the acid with the sample attenuated significantly (reaction indicated by bubbling) and there was no further significant change in pH observable, it was centrifuged to suck up most of the  $\text{H}_2\text{O}_2$  and water (Heraeus Cryofuge 8500i, Thermo Scientific) and freeze-dried afterwards (Sublimator 2-4-5, Zirbus Technology).

Less than 1 gram (g) of the sample (depending on the texture of the sample) was then weighed and filled into plastic bottles with a spoon sodium pyrophosphate and a one per cent diluted ammonia solution. The sodium pyrophosphate creates a mantle around each grain to impede agglutination of single grains. To ensure that all grains were separated from each other, the plastic bottles were put in a rotation shaker for at least one day (RS12 Rotoshake, Gerhardt).

Concerning the limitation of the grain size analysis, the measurements were restricted to grains smaller 1 millimetre (mm) removed mechanically with a 1-mm-sieve. The weight of the sieved grain fractions smaller and larger than 1 mm are obtained to determine how much of the grain fraction is not included in the grain size analysis (A1). This methodical error needs to be addressed accordingly and is indicated by the fractions larger than 1 mm in [wt%] removed with the sieve and the relative amount of grains ( $>1\text{mm}$ ) measured by the Mastersizer3000 (see Chapter 4.5).

To ensure a grain density obscuring the light between 2 and 15 %, a conic rotary sample divider (Laborette 27, Fritsch) divided the solution into 8 equally grain-distributed sub-samples. A sieve on top of the conic rotary sample divider filtered grains larger than 1 mm which were dried and weighed afterwards. The samples smaller than 1 mm were afterwards analysed with the grain size analyser (Malvern Mastersizer 3000 Hydro-LV).

The analysing device measured the light, obscured by the water in the tank beforehand, to calibrate the measurement of the grain size. The water level needed to be manually adjusted so that the grain density was within the obscuration range. At least three of the eight subsamples (from the rotary sampler) needed to be analysed. For each sample the device measured the GSD at least three times to ensure a statistical representation of the probe. The programme of the Malvern Mastersizer 3000 calculated averages, variances and deviation for each sample.

### 2.3.3 Ice content

After the thawing of the cylindrical or cubic samples, the water was extracted from the sample with a 5cm-Rhizon soil moisture sampler and a vacuum tube for further chemical analysis not included in this thesis (Figure 14). Out of 16 samples only seven were suitable for water extraction. The others did not contain sufficient water content for extraction. By applying the vacuum, water was sucked through the membrane of the Rhizon soil moisture sampler into the vacuum tube. In order to ensure that no air was drawn in and the Rhizon was fully submerged in the sample, the plastic bags were pressed together with tape. The samples after the extraction were freeze-dried to de-



*Figure 14: Setup of Rhizon soil moisture sampling in the AWI laboratories in Potsdam (Picture taken by Frieder Tautz)*

termine the total water content which was calculated from the difference in weight before and after the extraction and freeze-drying. Wet ( $\rho_w$ ) and dry ( $\rho_d$ ) bulk densities in [ $\text{g} * \text{cm}^{-3}$ ] were calculated using the respective wet ( $m_w$  in g) and dried ( $m_d$  in g) weight and the volume ( $V$ ) of the samples (Equation 1). The volume was obtained during subsampling in the cooling chamber by cutting cubes or cylinders out of the core and measuring these for their volumetric dimensions.

$$\rho = \frac{m}{V} \quad (1)$$

The volume of ice/water ( $V_i$  in  $\text{cm}^3$ ) in a sample was calculated with the difference in weight before ( $m_w$  in g) and after ( $m_d$  in g) removal of the water and an assumed ice density ( $\rho_i$  in  $\text{g} * \text{cm}^{-3}$ ) of  $0.9167 \text{ g} * \text{cm}^{-3}$  (Glen 1958) (Equation 2).

$$V_i = \frac{m_w - m_d}{\rho_i} \quad (2)$$

The ice content can also be calculated as volumetric ( $\theta$ ) with Equation 3 and gravimetric ( $u$ ) ice content with Equation 4 where  $V_g$  is the total volume of

the probe.

$$\theta = \frac{V_i}{V_g} * 100 \quad (3)$$

$$u = \frac{m_w - m_d}{m_d} * 100 \quad (4)$$

### 2.3.4 Soil Organic Carbon Content

With TOC values [wt%], the contribution of each layer ( $SOCC_{Layer}$ ) to the total SOCC of the profile can be retrieved with Equation 5 derived from Strauss 2014; Tamocai et al. 2009. The SOCC is the overall TOC [kilograms (kg)] per area unit [square metres ( $m^2$ )]. To obtain the SOCC at each site, the SOCC of all layers at the site are summed up. This calculation enables comparison between sites just for soil profiles with an equal amount of measurements or of soil profiles where sampling has been conducted for each soil horizon (1sub3 and Lake 11 - Position 4). T is the layer thickness in [m].

$$SOCC_{Layer} = \frac{TOC}{100} * \rho_d * 1000 * T \quad (5)$$

To enable comparison between all sites, each SOCC value per layer is reduced to the amount of SOCC per unit layer depth and is then averaged over all values of each profile (n is the number of observations). Multiplying it with the reference depth of 1 m calculates the averaged amount of SOCC per cubic metre soil [kg/cubic metres ( $m^3$ )] (Equation 6).

$$SOCC_{profile} = \frac{\sum (SOCC_{Layer}/T)}{n} * 100 \quad (6)$$

Since the dry bulk density ( $\rho_d$ ) is not acquired for every layer, it is average over the whole data set.

### 2.3.5 Radiocarbon dating

The age determination was conducted in the AWI laboratories in Bremerhaven, MICADAS<sup>3</sup> with the radiocarbon dating method ( $^{14}C$ ) on organic plant material making use of the radioactive decay of the carbon-14 isotope ( $^{14}C$ ) nuclide. There are three existing isotopes of C: carbon-12 isotope ( $^{12}C$ ), carbon-13 isotope ( $^{13}C$ ) and the most stable  $^{14}C$ . The  $^{14}C$  isotope originates from the reaction of stable nitrogen-14 isotope ( $^{14}N$ ) with solar neutrons in the upper troposphere and in the stratosphere and exhibit a certain propor-

<sup>3</sup><https://www.awi.de/en/science/geosciences/marine-geochemistry/micadas.html> [9.10.2020]

tion in the atmosphere (approximately one  $^{14}\text{C}$  atom per 1012 stable C atoms). Hence, they are part of the C cycle. Living organisms absorb and metabolise the C atoms through photosynthesis assimilating  $\text{CO}_2$ . After the organisms death the  $^{14}\text{C}$  nuclide decays into the more stable N at a constant rate and the ratio between  $^{14}\text{C}$  and  $^{12}\text{C}$  diminishes consequently. The radioactive half-life of  $^{14}\text{C}$ , the time after which half of the  $^{14}\text{C}$  atoms are decayed, amounts  $5730 \pm 40$  years (a) (Dawson and Brooks 2001; Godwin 1962). The corresponding time since the organisms death (t in a) can be calculated with equation 7 where the decay constant  $\lambda$  is in  $[\text{a}^{-1}]$ , the original  $^{14}\text{C}$  content ( $^{14}\text{C}_{t=0}$ ) and the  $^{14}\text{C}$  content after a certain time ( $^{14}\text{C}_{t=1}$ ) in [percent modern C] (Libby 1961; Stuiver and Polach 1977). The unit [percent modern C] is the  $^{14}\text{C}$  value from 1950 for the purpose of comparison of papers throughout history.

$$t = \frac{1}{\lambda} * \ln \frac{^{14}\text{C}_{t=0}}{^{14}\text{C}_{t=1}} \quad (7)$$

The method with the Accelerator Mass Spectrometer (AMS) determining the isotope ratios, has a detection limit of approximately 50.000 a (Fairbanks et al. 2005).

## 2.4 Statistical approach

All of the statistical analyses and visualisations are conducted with the programme R - Version 3.6.3 and LibreOffice Calc. Maps are created with QGIS OpenSource - Version 3.10.4 - A Coruña.

At two sites the ALT was not obtained due to the limits of the active layer probe (100 cm) used to assess the ALT, noted with a "larger than" sign. For the statistical analysis the value is set to the highest possible value, hence 100 cm.

The biochemical data was handled similarly. The devices accuracy is limited to its lowest value of 0.1 wt%. Any values below that are displayed accordingly ( $< 0.1$  wt%), yet it is set to exactly 0.1 wt% to include the values in the statistical analysis. The gravimetric percentage is transferred into a more useful unit of [g/kg] by multiplying the value [wt%] by 10. The difference between categories is determined by their mean.

The ALT has been acquired at more positions than otherwise included in the data set. The comparison of the ALT among sites includes additional ALT measurements acquired during the same expedition by Inge Grünberg, AWI. It is only used for plots concerning the ALT to ensure a higher number of values and hence a higher significance when making deductions. This data set includes ALT measurements at sites far away from any thaw slumps and the

definition of disturbance is not just restricted to thaw slump activity but it contains sites far away from any lakes and/or thaw slump activity (Chapter 1.3). When referring to other parameters than ALT, the data set is reduced to the number of samples analysed in the laboratories.

The  $^{14}\text{C}$  data analysed in the AWI laboratories in Bremerhaven needed to be calibrated according to the historical  $^{14}\text{C}/^{12}\text{C}$  ratio. The raw data from the laboratories are calculated with a constant historical ratio between those two isotopes in the atmosphere and hence a constant exchange between the vegetation and other reservoirs is falsely assumed. Different  $^{14}\text{C}$  archives have shown that the ratio has been highly variable over the course of time (Fairbanks et al. 2005; Libby 1961; Reimer et al. 2013; Stuiver and Polach 1977). This is why the radiocarbon age has been calibrated with the INTCAL13 data set from 2017 (Reimer et al. 2013).

Outliers in the boxplots were checked for potential sources of sampling errors in the data. Any disruption in the general horizontal layer structure, observed as outliers in the data, are removed from the statistical analysis. They indicate a vertical transportation of material and a clear processes of cryoturbation. To analyse any other processes apart from cryoturbation, vertical transportation of material needed to be identified and excluded since a cryoturbated ground features different values than a layered soil profile. The layers at Lake 6 - Position 1 (30-35 cm layer depth) and 1sub3 (70-80 cm layer depth), exhibiting cryoturbating characteristics visible in the pictures taken at the sites, are therefore excluded (Figures 15a and 15b). Any other outliers with no apparent reason for removal from the statistical analysis, remain in the data set. Outliers particularly discussed for exclusion are at Lake 11 - Position 4 (10-20 and 40-46 cm layer depth) and Position 6 (50-70 cm layer depth) but owing to lack of pictures or any other reason for removal, these values are to remain in the data set.

Measurements from AL and permafrost layers are compared to determine any differences between the permanently cryotic and the non-cryotic parts of the soil. Whenever the layer depth of a measurement (biochemistry, grain size) is relevant, the middle depth between the layer boundaries is determined. To find any pattern in the GSD, the layers with grain size measurements from the AL are categorised according to their layer depth. There are three categories introduced: 0-30 cm, 30-70 cm and 70-100 cm.

Tests of significance are performed with the Welch's two sample T-Test ( $\alpha = 0.05$ ). Correlation is calculated with Pearsons correlation coefficient  $r$ .



(a) The horizontal layer structure is disrupted due to cryoturbating processes [69.033713 North, 133.253683West] (Picture taken on 20th of August, 2018 by Julia Boike, AWI) Site: Lake 6 - Position 1.



(b) Although a horizontal structure can be determined, in particular in the lower part of the AL profile, irregularities are a sign of cryogenic processes [68.740759 North, 133.494441West] (Picture taken on 26th of August, 2018 by Julia Boike, AWI). Site: 1sub3

Figure 15: Soil profiles with visible cryotic processes indicated by the white line and arrow. Outliers occurring at the depths of these discontinuities are excluded from further statistical analysis.

## 3 Results

### 3.1 General properties

The 69 measurements are distributed over 13 different positions east of the Mackenzie Delta at 6 different sites. There are 34 AL and 35 permafrost measurements from a maximum depth of 1.22 m.

The gravimetric and volumetric ice content amounts on average 60.6 wt% and 73.0 volumetric percentage (vol%) respectively for the 16 samples obtained for ice content acquisition. The ice content in this study remains within the range of 36-81 wt% and 59-85 vol%. Most ice-content data were acquired at Lake 1, an undisturbed site in the proximity of a lake, featuring the highest values in the data set (Figure A2). The other four ice content measurements at 1sub3, TVC and Lake 6 - Position 2 are lower.

Soil profiles with no evident sign of permafrost disturbance (TVC and 1sub3) exhibit quite low ice content values similar to the only ice content measurement at a disturbed site (Lake 6 - Position 2). In general, the volumetric ice content decreases with increasing layer depth below the frost table ( $r = -0.64$ ).

The wet and dry bulk densities of the samples taken from the permafrost are on average 1.2 and 0.5  $\text{g} \cdot \text{cm}^{-3}$  respectively. Such as the ice content measurements, bulk densities were only obtained for permafrost cores but also

reside within the expected range for the NWT, Canada (Vardy et al. 2000).

The radiocarbon dating age of the layers vary between 678 and 42,860 calibrated radiocarbon years before present (cal. a BP) with an average of 14,662 cal. a BP (Table 2). There are no soil samples from the time period between 8,300 and 19,867 cal. a BP.

A vertical correlation ( $r = 0.697$ ) between layer depth and  $^{14}\text{C}$  values is observed. Just at Lake 6 - Position 2 the upper layer is older (17,398 cal. a BP) than the lower one (8,172 cal. a BP).

*Table 2: Radiocarbon age with according layer boundaries, their ALT and disturbance categories. The radiocarbon age is calibrated with the INTCAL13 data set from 2017 (Reimer et al. 2013) according to the historical  $^{14}\text{C}/^{12}\text{C}$  ratio. The range is  $2\sigma$  calculated with the R package "rcarbon". The table is sorted according to their site and their layer depths. NA = Not Available, LD = Layer depth, L = Lake, Pos = Position.*

Site	Upper LD [cm]	Lower LD [cm]	Radiocarbon age [cal. a BP]	Disturbance category	ALT [cm]
1sub3	50	60	3,665 - 3,684	no	85
1sub3	85	95	24,556 - 25,170	no	85
1sub3	107.5	109.5	32,802 - 33,457	no	85
L11 Pos4	50	70	5,461 - 5,584	yes	95
L11 Pos6	40	46	3,791 - 3,824	no	73
L11 Sim	70	100	26,642 - 27,246	yes	98
L12 Pos2	50	60	23,724 - 24,150	yes	74.5
L12 Pos3	70	80	19,867 - 20,217	yes	87
L12 Pos5	70	80	24,994 - 25,430	yes	NA
L12 Sim	70	90	42,553 - 43,175	yes	96
L1 Pos1	63	64.5	3,423 - 3,444	no	50
L1 Pos2	32	35.5	1,215 - 1,219	no	32
L1 Pos2	73	76.5	6,495 - 6,661	no	32
L6 Pos1	30	35	719 - 724	no	50
L6 Pos1	50	57	4,754 - 4,814	no	50
L6 Pos1	NA	NA	3,126 - 3,139	no	50
L6 Pos2	50	52	20,804 - 21,211	yes	50
L6 Pos2	70	75.5	8,259 - 8,300	yes	50
TVC	45	49	19,956 - 20,412	no	45

Table 3: Displaying the measurements of gravimetric and volumetric ice content in [wt%] and [vol%] respectively, the wet and dry bulk densities in  $[g * cm^{-3}]$  with their according volume when acquired in  $[cm^3]$ . Each measurement is accompanied with the layer boundaries, their according ALT and the disturbance category. Not every data point could be analysed for the aforementioned parameters to limited capacities. L - Lake, Pos - Position, TVC - Trail Valley Camp, c - core, al - active layer.

Site	Core/AL sample	Upper depth [cm]	Lower depth [cm]	ALT cm	Disturbance category	Grav. ice content [wt%]	Vol. ice content [vol%]	Wet bulk density $[g * cm^{-3}]$	Dry bulk density $[g * cm^{-3}]$	Volume $[cm^3]$
L1 Pos1	c1	50	52.5	50	no	58.3	77.2	1.2	0.5	2.12
L1 Pos1	c1	92	93	50	no	59.4	75.2	1.2	0.5	21.6
L1 Pos1	c1	63	64.5	50	no	78.3	84.8	1	0.2	8.23
L1 Pos1	c1	66	70.5	50	no	69.2	78.9	1	0.3	18.52
L1 Pos1	c1	76.5	79.5	50	no	66.8	71.7	1	0.3	10.95
L1 Pos1	c1	79.5	82.5	50	no	50.7	65.5	1.2	0.6	7.83
L1 Pos2	c2	32	35.5	32	no					
L1 Pos2	c2	35	39	32	no	65.4	77.51	1.1	0.4	18.29
L1 Pos2	c2	40	43	32	no	84.4	>90			
L1 Pos2	c2	43	47	32	no	71.9	83.4	1.1	0.3	36.1
L1 Pos2	c2	47	52	32	no	81.4	86.0	1	0.2	28.79
L1 Pos2	c2	65.5	69.5	32	no	60.3	76.3	1.2	0.5	57.89
L1 Pos2	c2	73	76.5	32	no	62.5	71.9	1.1	0.4	18.35
L6 Pos 1	al	30	35	35	no					
L6 Pos 1	al			35	no					
L6 Pos 1	c2	50	57	50	no					
L6 Pos 2	c1	50	52	50	yes					
L6 Pos 2	c1	70	75.5	50	yes	37.1	60.00	1.5	0.9	21.81
lsub3	al	50	60	85	no					
lsub3	c2	85	95	85	no					
lsub3	c2	98.5	101	85	no	35.8	59.2	1.5	1	17.87
lsub3	c2	107.5	109.5	85	no	40.5	61.0	1.4	0.8	13.22
TVC	c2	45	49	45	no	46.3	66.6	1.3	0.7	13.91
L11 Pos 6	al	40	46	73	no					
L11 Pos 4	al	50	70	95	yes					
L11 Pos Sim	al	70	100	98	yes					
L12 Pos 2	al	50	60	74.5	yes					
L12 Pos 3	al	70	80	87	yes					
L12 Pos 5	al	70	80	>98	yes					
L12 Pos Sim	al	70	90	96	yes					
<b>mean</b>				<b>56.98</b>		<b>60.6</b>	<b>73.01</b>	<b>1.19</b>	<b>0.51</b>	<b>19.70</b>

## 3.2 Biochemistry in active layer and permafrost

C contents vary in the whole data set (Appendix Table A1) between 4-300 g/kg TOC and 7-334 g/kg TC and have means of 44 g/kg TOC and 52 g/kg TC. C contents are significantly lower in the AL than in the cryotic ground ( $p < 0.05$ ) (Figure 16). Throughout the profiles there is on average four times as much TOC in the AL than in the permafrost (19 g/kg TOC in the AL compared to 78 g/kg TOC in permafrost). A similar difference is also observed with TC contents.

Most of the C values above the third quantile (51 g/kg for TOC and 56 g/kg for TC) are from permafrost measurements at Lake 1. Just two data points from Lake 6 feature values higher than the third quantile of TOC. The other sites have values below it.

TN values have an expected low mean of 2.3 g/kg TN (Broll et al. 1999; Vardy et al. 2000). Comparing measurements between AL and permafrost, TN contents in permafrost are 2.7 times higher in the AL (1.3 g/kg TN in the AL compared to 3.5 g/kg TN in permafrost ( $p < 0.05$ )). Similar to C, N values above the third quantile are mainly from Lake 1 and just two measurements from Lake 6.

The C/N ratio indicating the rate of mineralisation, is on average 14 in the AL and 20 in the permafrost. Although, it is significantly lower in the AL than in the permafrost ( $p < 0.05$ ), the C/N ratio varies greatly within a soil profile. Values as high as 21 occur in the AL (Lake 12 - Position 3) and the minimum of the N values in the whole data set of 4.2 is found in a permafrost sample at TVC.

## 3.3 Grain size distribution

All sites are mineral soils with averaged TOC contents below the threshold of 200 g/kg (Pries et al. 2012; Schuur et al. 2015). Some layers have TOC contents above 20 wt% but are restricted to sites with known Caccumulations in the cryotic ground (1sub3, Lake 6 - Position 1 and Lake 1 - Position 1 and 2) (Appendix Table A1).

The sand fraction is limited to grain sizes smaller than 1 mm due the laboratories restrictions and illustrates therefore not the complete picture. Detailed When categorising the fractions according to the layer depth of acquisition (Chapter 2.4), a tendency of downward migration of silt towards the lower layers is observed. There is a difference in silt fraction of 5 % between the upper 0.3 m and the lower 0.7-1 m (Figure 17 (b)). The clay fraction does not seem to be as prone to downward migration (Figure 17 (c)) and the mobili-

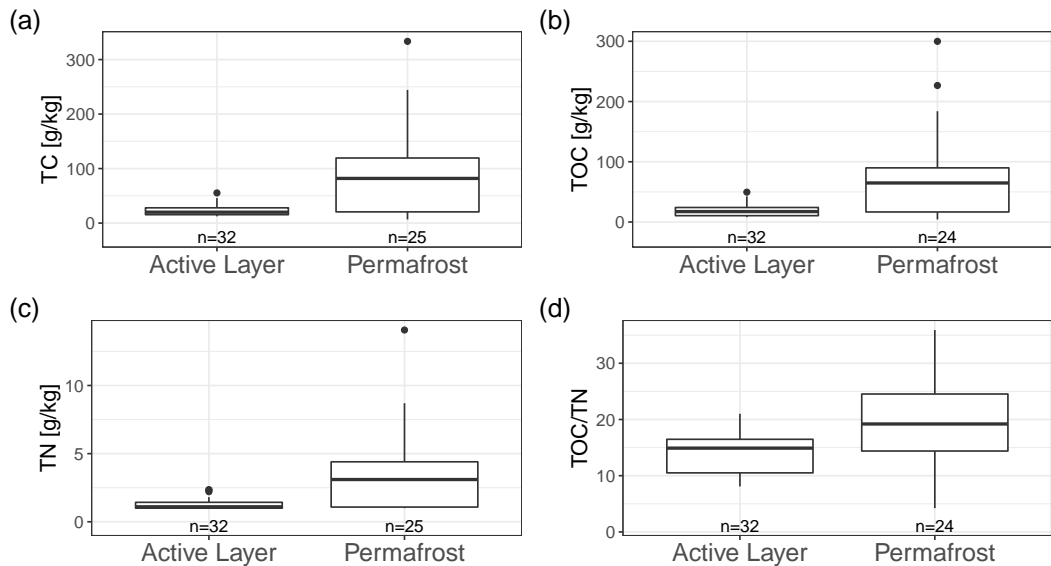


Figure 16: Comparison between AL and permafrost of TC, TOC, TN and C/N ratio. The AL shows a significant depletion of C and N due to microbial activity and an decreased C/N ratio indicating higher decomposition rates (Sollins et al. 1984; Stevenson 1994; Walthert et al. 2004).  $n$  is the number of observations.

sation of finer sediments in this study is mainly restricted to silt. The sand fraction increases where the silt is depleted (difference of 6 % between upper and lower layer category) (Figure 17 (a)).

Sites located directly at the headwall of thaw slumps (Lake 12 - Simon and Position 2, Lake 11 - Simon) show a negative correlation between the ratio of silt and the distance to the frost table (Pearson's  $r$  of -0.8312). Layers closer to the frost table have a higher silt fraction than layers further away from it. Sand on the other hand reveals a positive correlation at headwalls ( $r = 0.7653$ ). Enclosed soil profiles without any strong ablation areas seem not to be impacted by mobilising dynamics to a similar extent as the headwalls at thaw slumps.

The clay fraction does not show any apparent grain size differentiation within the soil profile according to the analysis.

### 3.4 Disturbance categories

This studies main focus lies on permafrost disturbance at thaw slumps in the proximity of lakes where thawing of permafrost is easily recognised (Chapter 1.3) and the threshold between disturbed and undisturbed ground is quite well distinguishable.

Of the extended data set regarding the ALT, 28 sites are categorised as undisturbed and 16 as disturbed totalling 45 sites suitable for comparison (Appendix Table A1 and Figure 18). Some sites are removed, because either positions

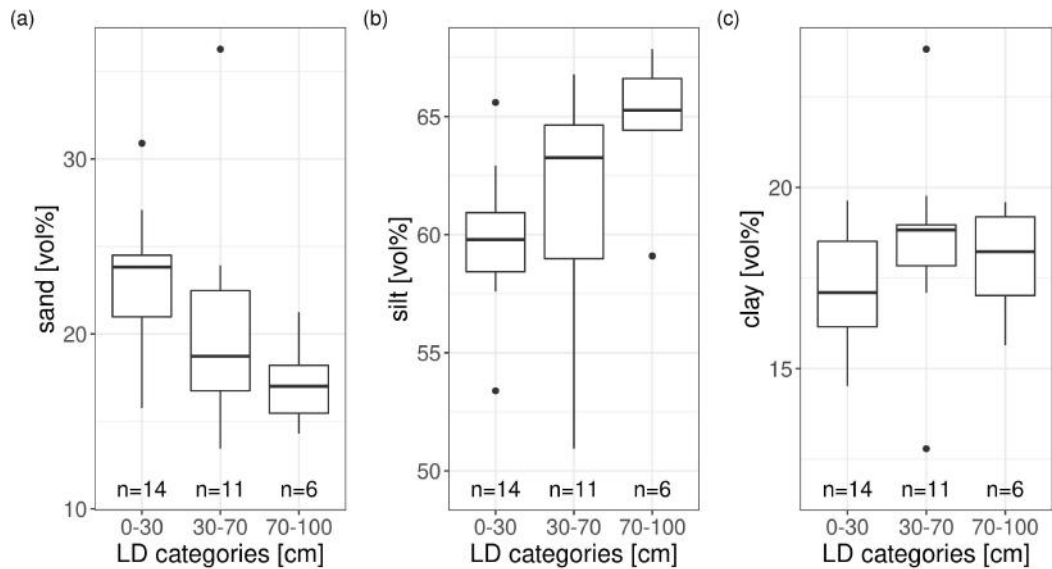


Figure 17: Grain size differentiation over the three depth categories of AL measurements. (a) sand, (b) silt and (c) clay fraction in [%]. The sand fraction is limited to grain sizes smaller 1 mm due to analytical restrictions of the laser (Chapter 2.4 and 4.5). LD = Layer depth

could not be assigned to one disturbance category with certainty or there are missing ALT measurements.

The ALT is 0.26 m at its thinnest and at its thickest more than the measurable one metre, and is expected to reach up to 2 m at disturbed sites (Brouchkov et al. 2004; Burn 1997; Nixon and Taylor 1998; Vardy et al. 1998). On average the ALT has a mean of 0.68 m. At undisturbed sites, it is significantly less (0.55 m) than at disturbed sites (0.91 m,  $p < 0.05$ ) (Figure 18) and has a difference of 0.36 m. Yet, there is a large variation of ALT among sites of the same disturbance category. Sites categorised as undisturbed may feature an ALT of up to 0.93 m (Lake 12 - Position 1 (Figure A10)) and sites categorised as disturbed may have an ALT of 0.26 m (Lake 6 ref - Position 2 (Figure A8)).

In the main data set, six sites are defined as undisturbed and seven as disturbed, whereof all disturbed sites are related to thaw slump activity. Most AL samples were taken from disturbed sites (26 compared to 6 samples) whereas most permafrost samples were obtained from undisturbed sites (29 compared to 6 samples).

Regarding C contents in the soil between disturbed and undisturbed sites, a significant difference of 72 g/kg TOC is observed ( $p < 0.05$ , Figure 19 (a) and (b)). That is 5.6 times the TOC content in undisturbed ground than in disturbed ground. A similar difference is visible in TC values.

TN is depleted to a similar extent (1.5 times in undisturbed ground, Figure 19). The C/N ratio is higher at disturbed sites with a differences in means

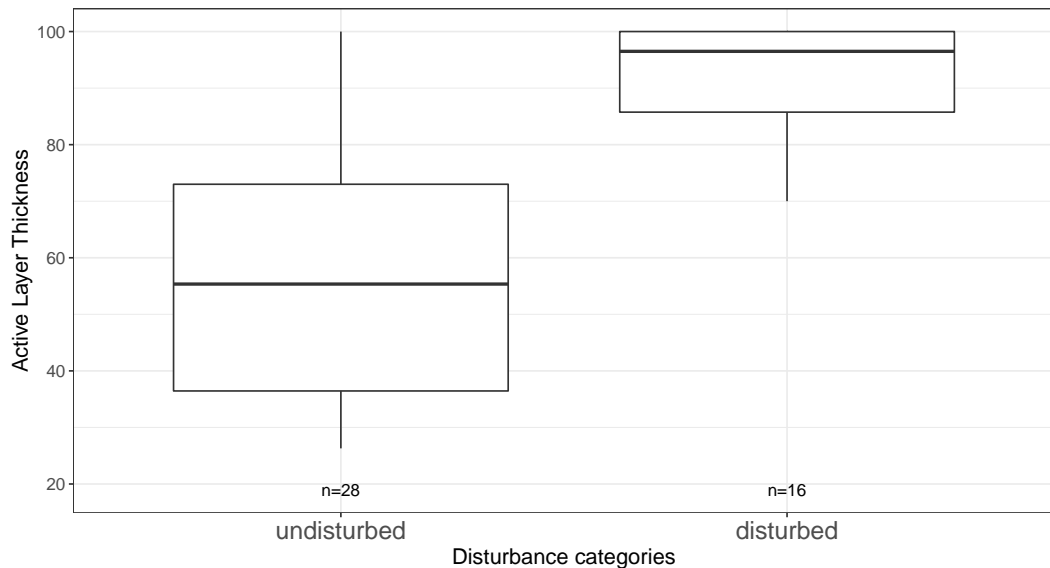


Figure 18: ALT measurements of disturbed and undisturbed sites. ALT is obtained from more sites ( $n = 42$ ) than otherwise included in this thesis ( $n = 13$ ) during the same expedition by Inge Grünberg, AWI. Some sites could not be categorised appropriately and were excluded from the analysis.

of 5.7 giving indications of the soils rate of mineralisation (Figure 19) (Sollins et al. 1984; Stevenson 1994; Walthert et al. 2004).

In this study, just two sites have similar amount of measurements and maximum layer depths (1sub3, undisturbed (Figure A5) and Lake 11 - Position 4, disturbed (Figure A4)). At site 1sub3 with an ALT of 0.85 m, some layers lie within the permafrost down to 1.1 m whereas at Lake 11 - Position 4 the layers are all within the AL of 0.95 m. Both sites consist of seven data points and are therefore suitable for comparison. The disturbed ground (Lake 11 - Position 4) exhibit a higher SOCC with  $8,1 \text{ kg/m}^2$  than the undisturbed ground (1sub3) with  $7,7 \text{ kg/m}^2$ . At site 1sub3 one value has been removed to reveal the influence of disturbance on the the SOCC on soils not being shadowed by potential cryoturbating processes (see Chapter 2.4). When this observation is included into the comparison, 1sub3 has a SOCC of  $30.7 \text{ kg/m}^2$  (compared to  $7.7 \text{ kg/m}^2$  without the outlier). Other sites are compared with averaged SOCC values with the calculation described in Chapter 2.3.4.

There is no significant difference between undisturbed and disturbed ground in averaged SOCC per unit layer depth and the values are highly variable independent on their disturbance categories ( $p\text{-value} > 0.05$ ) (Table 4). Comparison between sites are only possible by using the aforementioned averaged SOCC due to differing maximal layer depths at a give location and amount of measurements per site. Sites with a higher number of observations have in general an increased averaged SOCC since peak values in C content in the profile are more likely to be detected.

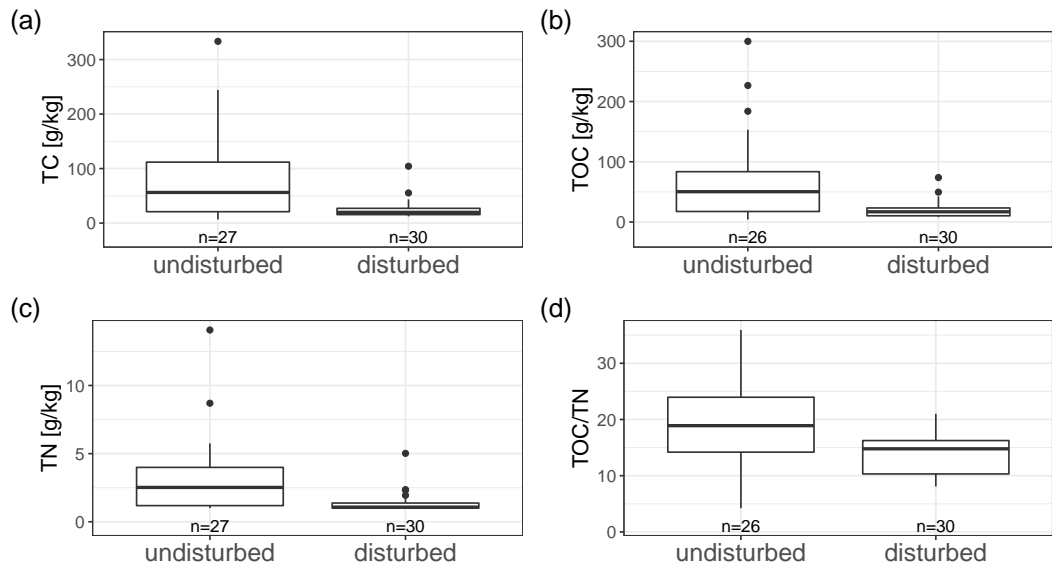


Figure 19: Difference of parameters at disturbed and undisturbed sites.  $n$  = number of observations, TOC = Total Organic Carbon, TC = Total Carbon, TN = Total Nitrogen, C/N ration = ratio between TOC and TN

The grain size distribution shows no clear distinction between disturbed and undisturbed ground (Figure 20). Although the soil does not loose grains to a notable extend at disturbed sites, the distribution within a soil profile may differ (Chapter 3.3).

Table 4: SOCC calculated for each site according to the method described in Chapter 2.3.4. Total SOCC values are difficult to compare with each other due to varying maximal layer depth. Averaged SOCC are used for this pupose. LD = Layer depth, no = undisturbed, yes = disturbed, L = Lake, Pos = Position, No. of obs. = Number of observations

Sites	Distur- bance	Averaged SOCC [kg/m <sup>3</sup> ]	LD [cm]	Total SOCC over profile [kg/m <sup>2</sup> ]	No. of obs.
L11Pos4	yes	0.09	90	8.41	8
L11Sim	yes	0.13	100	12.95	7
L12Pos2	yes	0.06	60	3.59	2
L12Pos3	yes	0.14	80	11	5
L12Pos5	yes	0.06	80	4.59	2
L12Sim	yes	0.05	100	4.58	4
L6Pos2	yes	0.17	87	15.18	2
1sub3	no	0.09	115	9.79	6
L6Pos1	no	0.25	58	14.78	10
L11Pos6	no	0.09	46	4.35	10
L1Pos1	no	0.54	94	50.46	3
L1Pos2	no	0.65	90	58.63	6
TVC	no	0.02	58	1.24	2

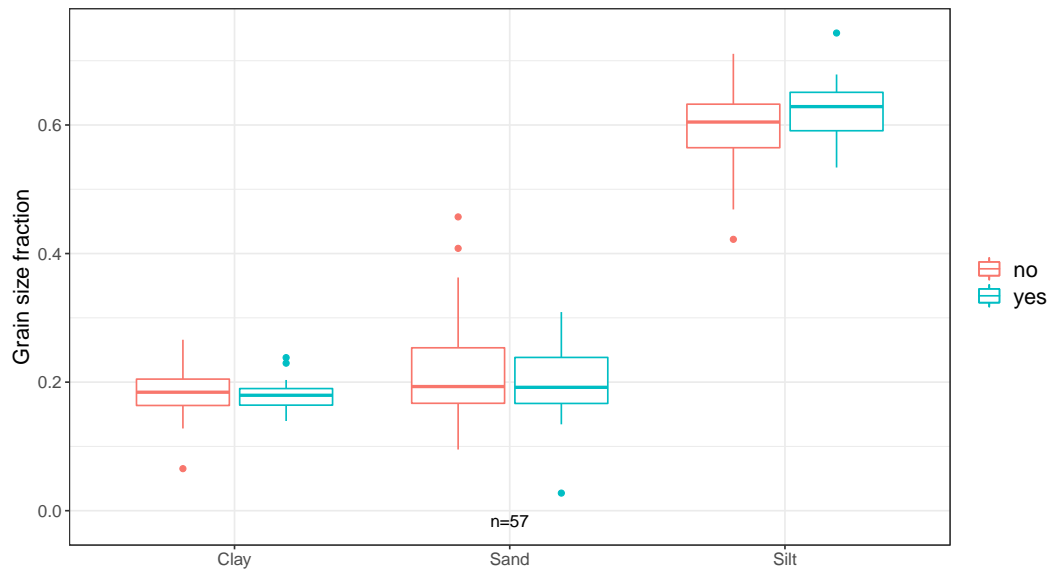


Figure 20: Grain size distribution of the whole data set between disturbed and undisturbed ground in the AL and the permafrost. The sand fraction is restricted to a size smaller 1 mm (see Chapter 2.3.2). yes - disturbed, no - undisturbed.

## 4 Discussion

General properties are consulted to compare them with other findings and reveal any outstanding characteristics. We found that ice accumulation areas are found close to the permafrost boundary and decrease with increasing layer depth below the frost table. In this study, the 14C age exhibit the typical vertical age structure having younger plant residues above older. The time gap without any 14C samples lies between 8,300 and 19,867 cal. a BP.

Comparison of parameters between the AL and the permafrost are utilised to reveal processes in regard of permafrost thaw. When permafrost thaws, the soil parameters may change to similar values observed in the AL- The biochemical values are highest in the permafrost and show a significant decrease in the AL. The C/N ratio is wider in the permafrost compared to the AL but has a strong site-specific variability. The silt fraction differs significantly at headwalls but the GSD features otherwise no clear differentiation between disturbed and undisturbed ground.

At disturbed sites, the ALT is increased, TOC, TC and TN values are lower, but the comparison of SOCC between two sites reveal an increase of SOCC at disturbed sites.

## 4.1 General Properties

Ice content is well within the expected magnitude in ice-rich permafrost in NWT, Canada. The values show a high variability within a soil profile and among sites, but there is a lack of peak values as observed in other studies (Bockheim 2007; Broll et al. 1999; Burn and Michel 1988; Kokelj and Burn 2003, 2005; Kokelj et al. 2002; Lacelle et al. 2004; Mackay 1983; Vardy et al. 2000). The soil might have experienced a loss of moisture during the Holocene warming period and further down higher values can be expected indicating relict active layer thicknesses (Burn 1997; Kokelj et al. 2002).

The ice content in the samples from the permafrost cores at Lake 1, 6, 1sub 3 and TVC show a significant variation across the landscape. Although the number of observation is not sufficient for thorough analysis of any pattern concerning permafrost degradation, the profiles at Lake 1 enable to draw some conclusions regarding water movement and accumulation in the soil.

The ice content at Lake 1 - Position 1 and 2 being highest 14.5 and 11 cm respectively underneath the frost table, indicate that ice accumulation occurs close to the frost table. Taking into account that the frost table varies annually and throughout the year according to prevailing climatic conditions (Hinkel and Nelson 2003; Nelson et al. 1998; Shiklomanov et al. 2016), the depth of accumulation is changing between years and the water accumulates at the deepest permafrost table depth (Kokelj and Burn 2003, 2005; Ping et al. 2008; Tarnocai and Bockheim 2011).

In contrast to these accumulation layers, the other sites have quite low ice content values (TVC, 1sub3 and Lake 6 - Position 2). Higher accumulation values can be expected but a low sample density at those sites does not reveal any layers of water accumulation.

The general vertical age structure may be disrupted by cryoturbating processes typical for permafrost soils (Bockheim 2007; Pries et al. 2012; Vandenberghe 2013). Layers with corresponding  $^{14}\text{C}$  ages show an increase in age in deeper layers. It is reversed at Lake 6 - Position 2 where cryoturbating processes are assumed by peak values in C content. An age difference of over 10,000 cal. a BP at this site between the top layer of the cryotic ground (layer depth of 0.52 m) and the 0.23 m lower layer measured for  $^{14}\text{C}$ , indicate that the current cryotic ground has been reworked in the past to a large degree. Having  $^{14}\text{C}$  ages from two different time periods in a reversed order display the degree of soil layer mixing possible in permafrost affected soils. Due to the proximity to a Lake, erosional processes in the past are likely and may have contributed to this pattern.

There appear to exist two major C accumulation periods when the soil func-

tioned as a C sink - one from ca. 8 ka ago during the mid-Holocene until the modern time period and the other over 20 ka ago, a time period residing within the late Pleistocene. Between those two periods the area is known to have been glaciated or covered by thick layers of snow (Dyke and Prest 1987; Murton 2009; Murton et al. 1997). Snow and ice covering the landscape impede the growth of plants and explain the lack of organic material from that time.

Plant residues from 20 ka ago are found at the sites Lake 6, 12, and TVC. Compared to other results with an assumed begin of glacial coverage ca. 22 ka ago (Burn and Kokelj 2009; Murton 2009), the findings in this study lead to the conclusion of a later coverage by glacier of this thesis' study area. These results may be explained by the altitude of the Caribou Hills where most of the sites lie within. The glacier may have covered the study area at a later date due to its elevated position compared to the Mackenzie Delta where the main ice flow occurred (Dyke and Prest 1987). Sharp escarpments south-west of the Caribou Hills might coincide with the movement of the Laurentide ice sheet along its edges. According to Burn and Kokelj (2009), Dyke and Prest (1987), and Murton (2009) large parts of the Mackenzie Delta and its margins were deglaciated ca. 12-17 ka ago but organic material has not commenced to accumulate before 8 ka ago - at least in this study area. Extended snow coverage and cold conditions might have prevented any significant grow of plants in that area. Like Pries et al. (2012) found, major accumulation of C leading to today's peak values, has occurred after the glaciation ca. 8 ka ago. That is why all TOC values larger than the mean of 44.38 g/kg TOC are from the time period younger than 8 ka.

## **4.2 Biochemistry in active layer and permafrost**

C values throughout the whole data set reflect typical C contents of mineral soils in arctic regions of North-America (Broll et al. 1999; Kokelj and Burn 2003; Kokelj et al. 2002; Vardy et al. 2000). Mineral soils are known to have significantly less C than organic soils (threshold of <200 g/kg TC) (Pries et al. 2012; Schuur et al. 2015) and TOC values below 50 g/kg are often observed in this study. In contrast to some studies where C contents decline with depth (Bockheim 2007; Broll et al. 1999; Kokelj and Burn 2003; Kokelj et al. 2002), in this study they vary greatly over the whole profile and do not show any correlation with increasing depth. C accumulation may be site-specific and varies across the landscape depending on various environmental factors affecting the amount of plant residues added to the soil and the degree of vertical translocation of OM. This may lead to the observed variety in the

data set.

In this study, there are just mineral soils with a high amount of consolidated materials (Chapter 3.3). They contain more C than fluvial sites by Broll et al. (1999) but do not show as high amounts as found in peatlands or hummocks (Kokelj and Burn 2003; Vardy et al. 2000).

The difference between C values from the permafrost and the AL (Figure 16) may be explained by higher microbial activity due to access to oxygen and higher temperatures.

In contrast, at the site 1sub3 there is 59 % less TOC in the permafrost than in the AL contradicting the hypothesis. In addition to a quite large ALT at an undisturbed site and indications for cryoturbation, the site 1sub3 may not be representative for typical undisturbed permafrost soils and features characteristic rather related to permafrost disturbance.

There is little N ( $< 10$  g/kg) in permafrost soils as other studies also found (Broll et al. 1999; Tarnocai and Bockheim 2011; Vardy et al. 2000). Most of the N is locked in the vegetation at the surface and decrease significantly with depth. Since the source of N is mainly organic material, high values are found in layers with high carbon content and vice versa.

Overall, the C/N ratio is significantly lower in the AL than in the permafrost due to higher decomposition of organic matter by microbes (Pries et al. 2012; Sollins et al. 1984; Stevenson 1994; Walthert et al. 2004).

Only one site has sufficient measurements from the AL and the permafrost (1sub3). Coincidentally, this is also a site identified for cryogenic process. When the data points with exceptional high values are removed (Chapter 2.4), the difference between AL and permafrost measurements of TOC is 14 g/kg for 1sub3 where the AL constitutes the higher value contradicting the hypothesis. Compared to the high difference among all sites (59 g/kg), this result suggests that the difference between AL and permafrost is not as high as otherwise shown in the data. A strong interconnection between cryotic and non-cryotic ground at a given site and a high variability between sites regarding C content profiles suggest using a different approach apart from comparison of means (Burn 1997; Kokelj et al. 2002; Lacelle et al. 2004; Osterkamp and Gosink 1991). The local settings such as accumulation rate of organic matter or the magnitude of cryogenic processes but also the ALT, the height of the water table giving access to oxygen for microbes and the level of disturbance are determining and influence the dynamics at each site to different extents.

### 4.3 Grain size distribution

Other studies do not show any or quite different differentiation patterns in the GSD (Broll et al. 1999; Kokelj and Burn 2003). The GSD within a soil profile occurs mainly at the silt level and is well observable at headwalls where mobilising processes seem to have an effect presumably by percolating meltwater at the exposed wall. The process of mobilisation of silt has been described before developing silt caps and silt-enriched layers (Locke 1986; Tarnocai and Bockheim 2011), but to a larger degree than observed in this study.

Clay and sand show no translocation downwards in the soil and seem to remain immobilised in the soil. Yet, sand is increased in upper layers due to the fact that the grain size distribution is calculated in fractions and the removal of one fraction leads to the increase of another fraction. Its immobile characteristic in well-drained, coarse-grained soils in the arctic has been described before (Locke 1986).

In contrast, clay does not show a similar behaviour as sand. This leads to the conclusion that clay is also susceptible to mobilisation just to a lesser extent than silt but is statistically shadowed by the fact that the GSD is shown in fractions and not in absolute numbers.

Moreover, the sand fraction has been mentioned as being an indicator for frost sorting (Corte 1961, 1962, 1963; Kaplar 1965; Locke 1986) and the data shows little sorting of the sand fraction implying little frost heave activity.

Apart from GSD at exposed headwalls, which show a clear mobilisation of silt, other profiles do not show any significant translocation of consolidated material and only reveal small tendencies in enclosed soil profiles.

### 4.4 Disturbance categories

Disturbance categories are introduced to examine parametrical differences in the soil between disturbed and undisturbed permafrost ground. The categorisation is based on mere personal experience and impression and is not based on any data so far.

Since the ALT data set is extended by additional measurements from the same expedition and includes disturbed categorised sites far away from any thaw slump activity such as most of the vegetation sites, to assign the sites to the categories is more complex (Table A1). Using only sites in the proximity of lakes and thaw slumps where the disturbance assignation is more perspicuous, the difference between disturbed and undisturbed sites show the same tendency towards increasing ALT at disturbed sites (0.34 m compared to 0.36 m of the extended data set).

Marsh et al. (2010) characterises the area with an ALT between 0.3 to 0.8 metre, yet at undisturbed sites. All of the ALT measurements in this study larger 0.9 m were taken at disturbed sites where ALT is expected to be increased (Brouchkov et al. 2004; Burn 1997; Lacelle et al. 2010; Lantz et al. 2009; Nixon and Taylor 1998; Vardy et al. 1998). Permafrost degradation is related to ground ice thawing and is therefore directly linked to the dynamics of the ALT.

Nonetheless, the variation between sites of the same disturbance category show that not only the magnitude of disturbance dictate an increasing ALT but other determining characteristics such as soil moisture, ground cover, the insulating effect of snow and organic matter or the non-conductive heat transfer between different media in the arctic tundra, may have an impact on the dynamics of thawing permafrost and thus increasing ALT (Biskaborn et al. 2019; Burn 2002; Hinkel and Nelson 2003; Nelson et al. 1998; Osterkamp 2007b; Shiklomanov et al. 2016; Vonk et al. 2015; Zhang and Stamnes 1998). Many sites in this study are also located in the proximity of lakes, where the lateral impact of disturbances might extend further than previously thought and undisturbed categorised positions are also affected by disturbance (Burn 2002; Grosse et al. 2011).

Increased microbial activity due to thickening AL, warmer ground temperatures, declined water table and new C reservoirs accessible to microbial decomposition at disturbed sites, explain the lower amount of sequestered C and N, which is released as GHG into the atmosphere indicating a contribution to global warming (see Chapter 1.1.2) (Burn 2011; Grosse et al. 2011; Lantuit et al. 2012; Schuur et al. 2015; Strauss et al. 2017). Similar conclusions are drawn from a wider C/N ratio at disturbed sites giving indications about the rate of mineralisation in the soil and the potential for further GHG release.

Previous studies of SOCC in the same study area or of comparable soils in North-America exhibit on average values higher 20 kg/m<sup>2</sup> in the first metre of the soil (Bockheim 2007; Grosse et al. 2011; Tamocai et al. 2009). A highly fluctuating C across the landscape and significant differences between cryotic and non-cryotic ground has been observed in these studies as well, but unlike in this study, values lower than 10 kg/m<sup>2</sup> SOCC in the first metre, as found at Lake 1 and at Lake 6 - Position 1, seem to be rare in continuous permafrost areas.

Comparing the two sites 1sub3 and Lake 11 - Position 4, unlike hypothesised, the SOCC in disturbed ground is higher than in the undisturbed ground. 1sub3 has one outlier removed before the calculation due to cryoturbating processes shadowing any processes regarding permafrost disturbance (Chapter 2.4). This difference shows, that accumulation layers are determining and may

be just detected with a finer sample resolution taken per soil profile. However, huge C accumulation layers when discovered, are excluded in this study to reveal general tendencies without the process of cryoturbation (Chapter 2.4). Other sites in this study are not comparable regarding total SOCC values due to unequal maximum layer depth or amount of measurements. Comparison between categories across the landscape is conducted with averaged SOCC per unit layer depth (Table 4).

Although there is no significant difference between the disturbance categories concerning averaged SOCC, certain sites stand out concerning SOCC values. At Lake 1 both positions exhibit values three times larger than at any other site. Together with the otherwise low values below  $5 \text{ kg/m}^2$ , the data reveal a highly fluctuating amount of SOCC in the soil regardless of their disturbance category and quite low values compared to other findings (Bockheim 2007; Grosse et al. 2011; Tamocai et al. 2009).

Reducing Soil Organic C stocks have been described but the data suggest that its development is strongly dependent on site-specific settings hindering prediction of future dynamics.

## 4.5 Limitations and errors

There are some limitations and errors traced back to the chosen methods in the laboratories and the subsequent statistical analysis. They are sometimes necessary and must be mentioned to understand the reliability and significance of the deduced conclusions.

Sampling in-situ and in the laboratories may have been preferential because of the equipments restrictions and the methods requirements. For instance, the grain size analysis required a relatively small amount of the soil sample for conducting the measurements and the device could not analyse grains  $> 1 \text{ mm}$ . Grains such as pebbles existing in the soil, have therefore not been included into the analysis. Similarly,  $^{14}\text{C}$  uses only a tiny portion of the samples for estimating its age. Assuming a soil mixing by cryoturbation and permafrost degradation, differing ages in the same layer may have been overseen and not been analysed. Outer parts of the cores and some AL samples have been thawed indicating an interruption in the cooling chain.

General properties have not been acquired in large amounts since they are only used to frame them into existing studies. Though, data used for further statistical analysis are therefore a crucial point were averaged values such as the bulk density, are computed to enable further estimations.

SOCC values are averaged over the whole soil profile and multiplied with the total layer depth. Major accumulation layers are therefore statistically shad-

owed by using the average or not even discovered owing to a low sampling resolution. As described in Chapter 4.4, single layers exhibit huge C accumulation and contribute to a great extent to the total SOCC in the soil.

Processes currently observed are expected to have occurred at larger depth during the Holocene warming interval as well. Cryogenic processes, previous mass movements or water percolation through the current cryotic layers sampled in this study, may have reached further down and lead to accumulation layers of C or ice and grain size differentiation at larger depth. Those past processes cannot be determined with this data set since the maximum layer depth of 1.2 m does not exceed the expected relict active layer thickness from over 8000 a ago which might have been up to 2.5 times thicker than today. Hence, the analysis of differences between AL and permafrost is restricted to the present ALT and strongly influenced by the polycyclisity of processes occurring in permafrost soils. The impact of paleoenvironmental conditions on present soil dynamics has still to be kept in mind and its contribution to the current state has to be accounted for. In addition, disturbed sites may have just recently started to experience permafrost degradation enlarging the expanse of the AL. Thus, the patterns have not yet evolved completely and are just marginally observable due to its juvenile nature.

Concerning the grain size distribution, the measuring device (Mastersizer3000) measured grains larger than 1 mm such as long and thin grains fitting through the sieve. It assumes a perfect spherical shape of the grains and obtains therefore grain size fractions larger 1 mm. Data for each individual site is displayed in the appendix (Table A1).

On average, 1 wt% but as much as 9 wt% of a whole sample can be excluded by this methodical limitation from further analysis (21).

When evaluating the grain size distribution of the AL samples taken in the field and the samples taken from the core, it has to be noted that the grains larger 1 mm, not fitting through the sieve, are not included in the analysis. Nevertheless, the grain size distribution obtained with the Mastersizer3000 exhibit a significant fraction larger than 1 mm.

On average, 8 vol% of a sample is measured as grains larger 1 mm, despite the mechanical removal by a sieve. As much as 25.8 vol% of a sample can contain these large grains. Comparing values of the grains obtained beforehand by mechanical removal in wt% and afterwards by the Mastersizer3000 in vol%, show that despite the removal of the larger grains, the measuring device still includes quite a large fraction of grains larger 1 mm. Nevertheless, this constitutes a potential source of errors in grain size distribution.

Regarding classification with the aid of ALT, biochemical measurements,

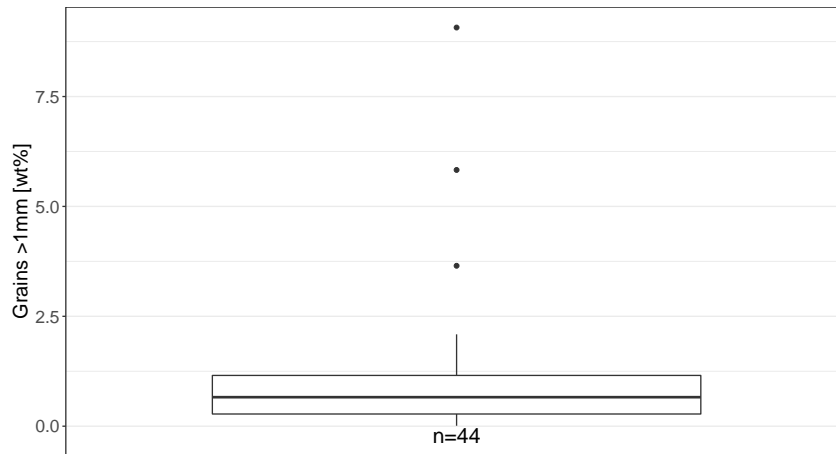


Figure 21: Boxplot of grains larger than 1 mm in [wt%] not included into the grain size analysis. This is a methodical error where grains larger than 1 mm were removed with a sieve. The plot shows the sand fraction larger than 1 mm in [wt%]. The outliers are at L1-Pos1 (4.94 wt% at 70-73 cm layer depth), 1sub3 (5.89 wt% at 98.5-101 cm layer depth) and L1 - Pos1 (9.3 wt% at 32-35.5 cm layer depth).

the results suggest an emendation of the disturbance definition. When microbes decompose organic material, the nutrient availability for plants increases and plants seem to have an increased growth (Chapter 1.3 (Li et al. 2017)). The enhanced plant growth has shown to be a reliable indicator but is no prerequisite for categorising permafrost disturbance. Disturbances may be occurring at sites without any visible signs. Site 1sub3 has indications of disturbance with an increased ALT and declined C contents.

Moreover, comparison between values from the cryotic and non-cryotic ground and between disturbance categories is biased because of an unequal distribution of samples from the cryotic and non-cryotic part of the soil. Out of 37 undisturbed categorised samples, 29 are taken from the cryotic ground whereas out of 32 disturbed categorised samples, 26 are acquired from the AL. When comparing these, the results are clearly biased by this preferential sampling setup.

## 5 Conclusion

General properties show that the sites exhibit typical permafrost soil features but do not show similar peak values in ice content as found by other studies. The  $\delta^{14}\text{C}$  values suggest a different glacial history for the study area than described for the Mackenzie Delta further east. The occurrence of  $\delta^{14}\text{C}$  values within the time period when glaciers were thought to cover the NWT, Canada entirely, suggest a later coverage of the study area.

Biochemical values between the cryotic and non-cryotic ground confirm the hypothesis of decreased values in the AL due to increased microbial activity and uptake of plants. Yet, depending on site-specific environmental factors impacting the soils composition and development, each soil profile may feature a different course regarding GHG release and degree of disturbance.

The GSD within the AL shows no significant differentiation by mobilising mechanisms. Just headwalls exhibit a clear mobilisation of the silt fraction downwards where exposition of permafrost ablates large amounts of material and the thaw slump enlarges.

Disturbed permafrost ground has an expected increased ALT and a decreased amount of TOC, TC and TN.

Together with the SOCC values, the data indicate that the introduced disturbance categories consist of highly fluctuating soil parameters, in particular in regard of C content. Disturbed categorised sites often show shallow ALT and have sometimes higher C content compared to undisturbed categorised sites contradicting expectations. As mentioned before, site-specific characteristics are quite crucial when analysing how the soil is impacted by permafrost disturbance and whether or not thermokarsts develop.

## 6 Acknowledgment

My first and foremost thanks go to Julia Boike. She has shown more patience with me than I could ever imagined. Within my options and my need for freedom regarding time scheduling, I was able to organise myself according to my liking without too much pressure from her. Simultaneously, she was able to give me the feedback I needed to understand what scientific writing demands. My insights into it could not have been better and more helpful for my future career.

Another thanks goes to the working group SPARC who endured my questions and often chaotic way of presenting my results: Niko Bornemann, Inge Grünberg, Stephan Lange, Jan Nitzbon and Bill Cable.

Well, and lastly my gratitude is addressed to my family - always supportive, always challenging and always there.

Thank you!

## 7 Eidesstattliche Erklärung

Hiermit versichere ich an Eides statt, dass ich die vorliegende Arbeit ohne fremde Hilfe angefertigt und keine anderen als die angegebenen Quellen und Hilfsmittel benutzt habe. Alle Teile, die wörtlich oder sinngemäß einer Veröffentlichung entstammen, sind als solche erkennbar. Die Arbeit wurde noch nicht veröffentlicht und auch noch keiner anderen Prüfungsbehörde vorgelegt.

Potsdam, den October 12, 2020

Unterschrift:

## References

- Akerman, H. J. (2005). “Relations between slow slope processes and active-layer thickness 1972-2002, Kapp Linné, Svalbard”. In: *Norsk Geografisk Tidsskrift* 59.2, pp. 116–128. DOI: [10.1080/00291950510038386](https://doi.org/10.1080/00291950510038386).
- Biskaborn, B. K. et al. (2019). “Permafrost is warming at a global scale”. In: *Nature Communications* 10.1, p. 264. ISSN: 2041-1723. DOI: [10.1038/s41467-018-08240-4](https://doi.org/10.1038/s41467-018-08240-4).
- Black, R. F. (1954). “Permafrost: A review”. In: *Bulletin of the Geological Society of America*. ISSN: 19432674. DOI: [10.1130/0016-7606\(1954\)65\[839:PR\]2.0.CO;2](https://doi.org/10.1130/0016-7606(1954)65[839:PR]2.0.CO;2).
- Bockheim, J. G. (2007). “Importance of Cryoturbation in Redistributing Organic Carbon in Permafrost-Affected Soils”. In: *Soil Science Society of America Journal* 71.4, pp. 1335–1342. ISSN: 0361-5995. DOI: [10.2136/sssaj2006.0414n](https://doi.org/10.2136/sssaj2006.0414n).
- Bockheim, J. G. and C. Tarnocai (1998). “Recognition of cryoturbation for classifying permafrost-affected soils”. In: *Geoderma* 81.3-4, pp. 281–293.
- Broll, G., C. Tarnocai, and G. Mueller (1999). “Interactions between vegetation, nutrients and moisture in soils in the Pangnirtung Pass Area, Baffin Island, Canada”. In: *Permafrost and Periglacial Processes* 10.3, pp. 265–277. ISSN: 10456740. DOI: [10.1002/\(SICI\)1099-1530\(199907/09\)10:3<265::AID-PPP326>3.0.CO;2-K](https://doi.org/10.1002/(SICI)1099-1530(199907/09)10:3<265::AID-PPP326>3.0.CO;2-K).
- Brouchkov, A., M. Fukuda, A. Fedorov, P. Konstantinov, and G. Iwahana (2004). “Thermokarst as a short-term permafrost disturbance, Central Yakutia”. In: *Permafrost and Periglacial Processes* 15.1, pp. 81–87. ISSN: 10456740. DOI: [10.1002/ppp.473](https://doi.org/10.1002/ppp.473).
- Brown, R. J.E. and W. O. Kupsch (1974). *Permafrost terminology*. Tech. rep. Tech. Memo. 111.
- Burn, C. R. (1997). “Cryostratigraphy, paleogeography, and climate change during the early Holocene warm interval, western Arctic coast, Canada”. In: *Canadian Journal of Earth Sciences* 34.7, pp. 912–925.
- (2002). “Tundra lakes and permafrost, Richards Island, Western Arctic coast, Canada”. In: *Canadian Journal of Earth Sciences* 39.8, pp. 1281–1298. ISSN: 00084077. DOI: [10.1139/e02-035](https://doi.org/10.1139/e02-035).
- (2011). “The thermal regime of a retrogressive thaw slump near Mayo, Yukon Territory”. In: *Canadian Journal of Earth Sciences* 37.7, pp. 967–981. ISSN: 0008-4077. DOI: [10.1139/e00-017](https://doi.org/10.1139/e00-017).
- Burn, C. R. and P. A. Friele (1989). “Geomorphology, vegetation succession, soil characteristics and permafrost in retrogressive thaw slumps near Mayo, Yukon Territory”. In: *Arctic* 42.1, pp. 31–40. ISSN: 00040843. DOI: [10.14430/arctic1637](https://doi.org/10.14430/arctic1637).

- Burn, C. R. and S. V. Kokelj (2009). “The environment and permafrost of the Mackenzie Delta area”. In: *Permafrost and Periglacial Processes* 20.2, pp. 83–105. ISSN: 10456740. DOI: [10.1002/ppp.655](https://doi.org/10.1002/ppp.655).
- Burn, C. R. and F. A. Michel (1988). “Evidence for recent temperature-induced water migration into permafrost from the tritium content of ground ice near Mayo, Yukon Territory, Canada”. In: *Canadian Journal of Earth Sciences*. ISSN: 00084077. DOI: [10.1139/e88-087](https://doi.org/10.1139/e88-087).
- Chapin, F. S., P. A. Matson, and H. A. Mooney (2002). *Principles of Terrestrial Ecosystem Ecology*. DOI: [10.1007/b97397](https://doi.org/10.1007/b97397).
- Chin, K. S., J. Lento, J. M. Culp, D. Lacelle, and S. V. Kokelj (2016). “Permafrost thaw and intense thermokarst activity decreases abundance of stream benthic macroinvertebrates”. In: *Global change biology*. DOI: [10.1111/gcb.13225](https://doi.org/10.1111/gcb.13225).
- Clark, P. U., A.S. Dyke, J. D. Shakun, A.E. Carlson, J. Clark, B. Wohlfarth, J.X. Mitrovica, S. W. Hostetler, and A. M. McCabe (2009). “The Last Glacial Maximum”. In: *Science* 325.5941, pp. 710–714. ISSN: 00368075. DOI: [10.1126/science.1172873](https://doi.org/10.1126/science.1172873).
- Corte, A. E. (1961). “The frost behavior of soils: laboratory and field data for a new concept. part 1, vertical sorting”. In:  
 — (1962). *The frost behavior of soils: laboratory and field data for a new concept. Part II: horizontal sorting*. Tech. rep. COLD REGIONS RESEARCH and ENGINEERING LAB HANOVER NH.  
 — (1963). “Particle sorting by repeated freezing and thawing”. In: *Science* 142.3591, pp. 499–501.
- Dawson, T. E. and P. D. Brooks (2001). “Fundamentals of Stable Isotope Chemistry and Measurement”. In: DOI: [10.1007/978-94-015-9841-5\\_1](https://doi.org/10.1007/978-94-015-9841-5_1).
- Dixon, J., J. R. Dietrich, and D. H. McNeil (1992). “Upper Cretaceous to Pleistocene sequence stratigraphy of the the Beaufort-Mackenzie and Banks Island areas, northwest Canada”. In: *Bulletin - Geological Survey of Canada*. DOI: [10.4095/133237](https://doi.org/10.4095/133237).
- Dyke, A. S. and D. J. A. Evans (2014). “Ice-marginal terrestrial landsystems: Northern laurentide and innuitian ice sheet margins”. In: *Glacial Landsystems*, pp. 143–163. ISBN: 9780203784976. DOI: [10.4324/9780203784976](https://doi.org/10.4324/9780203784976).
- Dyke, A. S. and V. K. Prest (1987). “Late Wisconsinan and Holocene history of the Laurentide Ice Sheet”. In: *Geographie Physique et Quaternaire* 41.2, pp. 237–263. ISSN: 07057199. DOI: [10.7202/032681ar](https://doi.org/10.7202/032681ar).
- Everdingen, R. O. van (1998). *Glossary of Permafrost and Related Ground-Ice Terms*. Vol. 21. 2, p. 213. ISBN: 0660125404. DOI: [10.2307/1551636](https://doi.org/10.2307/1551636). arXiv: [269-291](https://arxiv.org/abs/269-291).

- Fairbanks, R. G., R. A. Mortlock, T.C. Chiu, L. Cao, A. Kaplan, T. P. Guilderson, T. W. Fairbanks, A.L. Bloom, P. M. Grootes, and M. J. Nadeau (2005). “Radiocarbon calibration curve spanning 0 to 50,000 years BP based on paired  $^{230}\text{Th}/^{234}\text{U}/^{238}\text{U}$  and  $^{14}\text{C}$  dates on pristine corals”. In: *Quaternary Science Reviews*. ISSN: 02773791. DOI: [10.1016/j.quascirev.2005.04.007](https://doi.org/10.1016/j.quascirev.2005.04.007).
- French, H. M. (2013). *The periglacial environment: Third edition*. DOI: [10.1002/9781118684931](https://doi.org/10.1002/9781118684931).
- Glen, J. W. (1958). *The mechanical properties of ice I. The plastic properties of ice*. Tech. rep. 26. AMERICAN METEOROLOGICAL SOCIETY BOSTON MA, pp. 254–265. DOI: [10.1080/00018735800101257](https://doi.org/10.1080/00018735800101257).
- Godwin, H. (1962). “Half-life of radiocarbon”. In: *Nature*. ISSN: 00280836. DOI: [10.1038/195984a0](https://doi.org/10.1038/195984a0).
- Google Maps (2017). *Google Sat*. URL: <https://mt1.google.com/vt/lyrs=s%7B%5C%7Dx=%7B%5C%7D7Bx%7B%5C%7D7D%7B%5C%7Dy=%7B%5C%7D7By%7B%5C%7D7D%7B%5C%7Dz=%7B%5C%7D7Bz%7B%5C%7D7D>.
- Gooseff, M. N., A. Balsler, W. B. Bowden, and J. B. Jones (2009). “Effects of hillslope thermokarst in Northern Alaska”. In: *Eos* 90.4, pp. 29–30. ISSN: 00963941. DOI: [10.1029/2009E0040001](https://doi.org/10.1029/2009E0040001).
- Grosse, G. et al. (2011). “Vulnerability of high-latitude soil organic carbon in North America to disturbance”. In: *Journal of Geophysical Research: Biogeosciences* 116.3, pp. 1–23. ISSN: 01480227. DOI: [10.1029/2010JG001507](https://doi.org/10.1029/2010JG001507).
- Gruber, S. (2012). “Derivation and analysis of a high-resolution estimate of global permafrost zonation”. In: *Cryosphere* 6.1, pp. 221–233. ISSN: 19940416. DOI: [10.5194/tc-6-221-2012](https://doi.org/10.5194/tc-6-221-2012).
- Grünberg, Inge, Evan Wilcox, Simon Zwieback, Philip Marsh, and Julia Boike (2020). “Linking tundra vegetation, snow, soil temperature, and permafrost”. In: *Biogeosciences Discussions*, pp. 1–29. ISSN: 1810-6277. DOI: [10.5194/bg-2020-88](https://doi.org/10.5194/bg-2020-88).
- Gundelwein, A., T. Müller-Lupp, M. Sommerkorn, E. T.K. Haupt, E. M. Pfeifer, and H. Wiechmann (2007). “Carbon in tundra soils in the Lake Labaz region of arctic Siberia”. In: *European Journal of Soil Science* 58, pp. 1164–1174. ISSN: 13510754. DOI: [10.1111/j.1365-2389.2007.00908.x](https://doi.org/10.1111/j.1365-2389.2007.00908.x).
- Hinkel, K. M. and F. E. Nelson (2003). “Spatial and temporal patterns of active layer thickness at Circumpolar Active Layer Monitoring (CALM) sites in northern Alaska 1995–2000”. In: *Journal of Geophysical Research D: Atmospheres* 108.2, pp. 1995–2000. ISSN: 01480227. DOI: [10.1029/2001jd000927](https://doi.org/10.1029/2001jd000927).
- Hinkel, K. M., F. Paetzold, F. E. Nelson, and J. G. Bockheim (2001). “Patterns of soil temperature and moisture in the active layer and upper permafrost

- at Barrow, Alaska: 1993-1999”. In: *Global and Planetary Change* 29.3-4, pp. 293–309. ISSN: 09218181. DOI: [10.1016/S0921-8181\(01\)00096-0](https://doi.org/10.1016/S0921-8181(01)00096-0).
- Huang, J. et al. (2017). “Recently amplified arctic warming has contributed to a continual global warming trend”. In: *Nature Climate Change* 7.12, pp. 875–879. ISSN: 17586798. DOI: [10.1038/s41558-017-0009-5](https://doi.org/10.1038/s41558-017-0009-5).
- Hugelius, G. et al. (2014a). “Estimated stocks of circumpolar permafrost carbon with quantified uncertainty ranges and identified data gaps”. In: *Biogeosciences* 11.23, pp. 6573–6593. ISSN: 17264189. DOI: [10.5194/bg-11-6573-2014](https://doi.org/10.5194/bg-11-6573-2014).
- (2014b). “Estimated stocks of circumpolar permafrost carbon with quantified uncertainty ranges and identified data gaps”. In: *Biogeosciences* 11.23, pp. 6573–6593. ISSN: 17264189. DOI: [10.5194/bg-11-6573-2014](https://doi.org/10.5194/bg-11-6573-2014).
- IPCC (2013). *Climate Change 2013 - The Physical Science Basis. Fifth Assessment Report*. Tech. rep., p. 1535. DOI: [10.1017/CB09781107415324.004](https://doi.org/10.1017/CB09781107415324.004). arXiv: [arXiv:1011.1669v3](https://arxiv.org/abs/1011.1669v3).
- Kaplar, C. W. (1965). “Stone migration by freezing of soil”. In: *Science* 149.3691, pp. 1520–1521.
- King, A. W., L. Dilling, G. P. Zimmerman, D. M. Fairman, R. A. Houghton, G. Marland, A. Z. Rose, and T. J. Wilbanks (2008). *The first state of the carbon cycle report (SOCCR): The North American carbon budget and implications for the global carbon cycle*. Tech. rep., pp. 101–112.
- Kitover, D. C., R. T. van Balen, J. Vandenberghe, D. M. Roche, and H. Renssen (2016). “LGM Permafrost Thickness and Extent in the Northern Hemisphere derived from the Earth System Model iLOVECLIM”. In: *Permafrost and Periglacial Processes*. ISSN: 10991530. DOI: [10.1002/ppp.1861](https://doi.org/10.1002/ppp.1861).
- Kokelj, S. V. and C. R. Burn (2003). “Ground ice and soluble cations in near-surface permafrost, Inuvik, Northwest Territories, Canada”. In: *Permafrost and Periglacial Processes* 14.3, pp. 275–289. ISSN: 10456740. DOI: [10.1002/ppp.458](https://doi.org/10.1002/ppp.458).
- (2005). “Geochemistry of the active layer and near-surface permafrost, Mackenzie delta region, Northwest Territories, Canada”. In: *Canadian Journal of Earth Sciences* 42.1, pp. 37–48. ISSN: 0008-4077. DOI: [10.1139/e04-089](https://doi.org/10.1139/e04-089).
- Kokelj, S. V., R. E. Jenkins, D. Milburn, C. R. Burn, and N. Snow (2005). “The influence of thermokarst disturbance on the water quality of small upland lakes, Mackenzie Delta region, Northwest Territories, Canada”. In: *Permafrost and Periglacial Processes* 16.4, pp. 343–353. ISSN: 10456740. DOI: [10.1002/ppp.536](https://doi.org/10.1002/ppp.536).

- Kokelj, S. V. and M. T. Jorgenson (2013). “Advances in thermokarst research”. In: *Permafrost and Periglacial Processes* 24.2, pp. 108–119. ISSN: 10456740. DOI: [10.1002/ppp.1779](https://doi.org/10.1002/ppp.1779).
- Kokelj, S. V., T. C. Lantz, J. Kanigan, S. L. Smith, and R. Coutts (2009). “Origin and polycyclic behaviour of tundra thaw slumps, Mackenzie Delta region, Northwest Territories, Canada”. In: *Permafrost and Periglacial Processes* 20, pp. 173–184. ISSN: 10456740. DOI: [10.1002/ppp.642](https://doi.org/10.1002/ppp.642).
- Kokelj, S. V., T. C. Lantz, J. Tunnicliffe, R. Segal, and D. Lacelle (2017). “Climate-driven thaw of permafrost preserved glacial landscapes, northwestern Canada”. In: *Geology* 45.4, pp. 371–374. ISSN: 19432682. DOI: [10.1130/G38626.1](https://doi.org/10.1130/G38626.1).
- Kokelj, S. V., C. A.S. Smith, and C. R. Burn (2002). “Physical and chemical characteristics of the active layer and permafrost, Herschel Island, western Arctic Coast, Canada”. In: *Permafrost and Periglacial Processes* 13.2, pp. 171–185. ISSN: 10456740. DOI: [10.1002/ppp.417](https://doi.org/10.1002/ppp.417).
- Kokelj, S. V., J. Tunnicliffe, D. Lacelle, T. C. Lantz, K. S. Chin, and R. Fraser (2015a). “Increased precipitation drives mega slump development and destabilization of ice-rich permafrost terrain, northwestern Canada”. In: *Global and Planetary Change* 129, pp. 56–68. ISSN: 09218181. DOI: [10.1016/j.gloplacha.2015.02.008](https://doi.org/10.1016/j.gloplacha.2015.02.008).
- Kokelj, S. V., J. Tunnicliffe, Denis Lacelle, T. C. Lantz, and R. H. Fraser (2015b). “Retrogressive thaw slumps: From slope process to the landscape sensitivity of northwestern Canada”. In: *68e Conférence Canadienne de Géotechnique et 7e Conférence Canadienne sur le Pergélisol, 20 au 23 septembre 2015, Québec, Québec*. October.
- Koven, C. D. et al. (2015). “A simplified, data-constrained approach to estimate the permafrost carbon-climate feedback”. In: *Philosophical Transactions of the Royal Society A: Mathematical, Physical and Engineering Sciences*. ISSN: 1364503X. DOI: [10.1098/rsta.2014.0423](https://doi.org/10.1098/rsta.2014.0423).
- Kutzbach, L., P. Overduin, E.-M. Pfeiffer, S. Wetterich, and S. Zubrzycki (2010). “3. 3 Terrestrischer und submariner Permafrost in der Arktis”. In: *Warnsignal Klima: Das Eis der Erde*, pp. 78–86. DOI: [10.2312/warnsignal.klima.eis-der-erde.12](https://doi.org/10.2312/warnsignal.klima.eis-der-erde.12).
- Lacelle, D., J. Bjornson, and B. Lauriol (2010). “Climatic and geomorphic factors affecting contemporary (1950-2004) activity of retrogressive thaw slumps on the Aklavik plateau, Richardson mountains, NWT, Canada”. In: *Permafrost and Periglacial Processes* 21, pp. 1–15. ISSN: 10456740. DOI: [10.1002/ppp.666](https://doi.org/10.1002/ppp.666).
- Lacelle, D., J. Bjornson, B. Lauriol, I. D. Clark, and Y. Troutet (2004). “Segregated-intrusive ice of subglacial meltwater origin in retrogressive thaw flow head-

- walls, Richardson Mountains, NWT, Canada”. In: *Quaternary Science Reviews* 23.5-6, pp. 681–696. ISSN: 02773791. DOI: [10.1016/j.quascirev.2003.09.005](https://doi.org/10.1016/j.quascirev.2003.09.005).
- Lacelle, D., A. Brooker, R. H. Fraser, and S. V. Kokelj (2015). “Distribution and growth of thaw slumps in the Richardson Mountains-Peel Plateau region, northwestern Canada”. In: *Geomorphology* 235, pp. 40–51. ISSN: 0169555X. DOI: [10.1016/j.geomorph.2015.01.024](https://doi.org/10.1016/j.geomorph.2015.01.024).
- Lantuit, H. and W. H. Pollard (2005). “Temporal stereophotogrammetric analysis of retrogressive thaw slumps on Herschel Island, Yukon Territory”. In: *Natural Hazards and Earth System Science* 5.3, pp. 413–423. DOI: [10.5194/nhess-5-413-2005](https://doi.org/10.5194/nhess-5-413-2005).
- (2008). “Fifty years of coastal erosion and retrogressive thaw slump activity on Herschel Island, southern Beaufort Sea, Yukon Territory, Canada”. In: *Geomorphology* 95.1-2, pp. 84–102. ISSN: 0169555X. DOI: [10.1016/j.geomorph.2006.07.040](https://doi.org/10.1016/j.geomorph.2006.07.040).
- Lantuit, H., W. H. Pollard, N. Couture, M. Fritz, L. Schirrmeister, H. Meyer, and H. W. Hubberten (2012). “Modern and Late Holocene Retrogressive Thaw Slump Activity on the Yukon Coastal Plain and Herschel Island, Yukon Territory, Canada”. In: *Permafrost and Periglacial Processes* 23.1, pp. 39–51. ISSN: 10456740. DOI: [10.1002/ppp.1731](https://doi.org/10.1002/ppp.1731).
- Lantz, T. C. and S. V. Kokelj (2008). “Increasing rates of retrogressive thaw slump activity in the Mackenzie Delta region, N.W.T., Canada”. In: *Geophysical Research Letters* 35.6. ISSN: 00948276. DOI: [10.1029/2007GL032433](https://doi.org/10.1029/2007GL032433).
- Lantz, T. C., S. V. Kokelj, S. E. Gergel, and G. H. R. Henry (2009). “Relative impacts of disturbance and temperature: Persistent changes in microenvironment and vegetation in retrogressive thaw slumps”. In: *Global Change Biology* 15.7, pp. 1664–1675. ISSN: 13541013. DOI: [10.1111/j.1365-2486.2009.01917.x](https://doi.org/10.1111/j.1365-2486.2009.01917.x).
- Li, Fei et al. (2017). “Warming effects on permafrost ecosystem carbon fluxes associated with plant nutrients”. In: *Ecology*. ISSN: 00129658. DOI: [10.1002/ecy.1975](https://doi.org/10.1002/ecy.1975).
- Libby, W. F. (1961). “Radiocarbon dating”. In: *Science*. ISSN: 00368075. DOI: [10.1126/science.133.3453.621](https://doi.org/10.1126/science.133.3453.621).
- Locke, W. W. (1986). “Fine Particle Translocation in Soils Developed on Glacial Deposits, Southern Baffin Island, N.W.T., Canada”. In: *Arctic and Alpine Research* 18.1, pp. 33–43. ISSN: 00040851. DOI: [10.2307/1551212](https://doi.org/10.2307/1551212).
- Mackay, J. R. (1963). *Mackenzie Delta Area, NWT*. Department of mines and technical survey, Ottawa.

- Mackay, J. R. (1983). “Downward water movement into frozen ground, western arctic coast, Canada.” In: *Canadian Journal of Earth Sciences*. ISSN: 00084077. DOI: [10.1139/e83-012](https://doi.org/10.1139/e83-012).
- Margesin, R. (2009). *Permafrost Soils*. Vol. 16. Springer, Berlin, Heidelberg 2009. ISBN: 978-3-540-69370-3. DOI: [10.1007/978-3-540-69371-0](https://doi.org/10.1007/978-3-540-69371-0).
- Marsh, P., P. Bartlett, M. MacKay, S. Pohl, and T. Lantz (2010). “Snowmelt energetics at a shrub tundra site in the western Canadian Arctic”. In: *Hydrological Processes*. ISSN: 08856087. DOI: [10.1002/hyp.7786](https://doi.org/10.1002/hyp.7786).
- Marushchak, M. E., A. Pitkämäki, H. Koponen, C. Biasi, M. Seppälä, and P. J. Martikainen (2011). “Hot spots for nitrous oxide emissions found in different types of permafrost peatlands”. In: *Global Change Biology* 17.8, pp. 2601–2614. ISSN: 13541013. DOI: [10.1111/j.1365-2486.2011.02442.x](https://doi.org/10.1111/j.1365-2486.2011.02442.x).
- McGuire, A. D., L. G. Anderson, T. R. Christensen, S. Dallimore, L. Guo, D. J. Hayes, M. Heimann, T. D. Lorenson, R. W. Macdonald, and N. Roulet (2009). “Sensitivity of the Carbon Cycle in the Arctic to Climate Change”. In: *Ecological Monographs* 79.4, pp. 523–555.
- Morgenstern, A. (2012). “Thermokarst and thermal erosion : Degradation of Siberian ice-rich permafrost”. PhD thesis.
- Murton, J. B. (2001). “Thermokarst sediments and sedimentary structures, Tuktoyaktuk Coastlands, western Arctic Canada”. In: *Global and Planetary Change* 28.1-2, pp. 175–192. ISSN: 09218181. DOI: [10.1016/S0921-8181\(00\)00072-2](https://doi.org/10.1016/S0921-8181(00)00072-2).
- (2009). “Stratigraphy and palaeoenvironments of Richards Island and the eastern Beaufort Continental Shelf during the last glacial-interglacial cycle”. In: *Permafrost and Periglacial Processes* 20.2, pp. 107–125. ISSN: 10456740. DOI: [10.1002/ppp.647](https://doi.org/10.1002/ppp.647).
- Murton, J. B., H. M. French, and M. Lamothe (1997). “Late Wisconsinan erosion and eolian deposition, Summer Island area, Pleistocene Mackenzie Delta, Northwest Territories: Optical dating and implications for glacial chronology”. In: *Canadian Journal of Earth Sciences* 34.2, pp. 190–199. ISSN: 00084077. DOI: [10.1139/e17-015](https://doi.org/10.1139/e17-015).
- Nelson, F. E., S. I. Outcalt, J. Brown, N. I. Shiklomanov, and K. M. Hinkel (1998). “Spatial and Temporal Attributes of the Active-Layer Thickness Record, Barrow, Alaska, U.S.A.” In: *Permafrost - 7th international Conference*. 55, pp. 797–802.
- Nixon, F. M. and A. E. Taylor (1998). “Regional active layer monitoring across the sporadic, discontinuous and continuous permafrost zones, Mackenzie Valley, northwestern Canada”. In: *Proceedings of the Seventh International Conference on Permafrost* 55, pp. 815–820.

- Olefeldt, D. et al. (2016). “Circumpolar distribution and carbon storage of thermokarst landscapes”. In: *Nature Communications*. ISSN: 20411723. DOI: [10.1038/ncomms13043](https://doi.org/10.1038/ncomms13043).
- Osterkamp, T. E. (2007a). “Causes of warming and thawing permafrost in Alaska”. In: *Eos* 88.48, pp. 522–523. DOI: [10.1029/2007E0480002](https://doi.org/10.1029/2007E0480002).
- (2007b). “Characteristics of the recent warming permafrost in Alaska”. In: *Journal of Geophysical Research: Earth Surface* 112.2, pp. 1–10. ISSN: 21699011. DOI: [10.1029/2006JF000578](https://doi.org/10.1029/2006JF000578).
- Osterkamp, T. E. and J. P. Gosink (1991). “Variations in permafrost thickness in response to changes in paleoclimate”. In: *Journal of Geophysical Research: Solid Earth* 96.B3, pp. 4423–4434.
- Ping, C. L., J. G. Bockheim, J. M. Kimble, G. J. Michaelson, D. A. Walker, and F. Fliet-lanoe (1998). “Characteristics of cryogenic soils along a latitudinal transect in on permafrost by linear In the case of large-scale processes are subject one Classification Soils in review , Staff , freezing front as the active layer refreezes in the fall . Freezing Or”. In: *Journal of Geophysical Research* 103.D22, pp. 28, 917–28, 928.
- Ping, C. L., G. J. Michaelson, J. M. Kimble, V. E. Romanovsky, Y. L. Shur, D. K. Swanson, and D. A. Walker (2008). “Cryogenesis and soil formation along a bioclimate gradient in Arctic North America”. In: *Journal of Geophysical Research: Biogeosciences* 113.3. ISSN: 01480227. DOI: [10.1029/2008JG000744](https://doi.org/10.1029/2008JG000744).
- Pries, Caitlin E.Hicks, Edward A.G. Schuur, and K. Grace Crummer (2012). “Holocene Carbon Stocks and Carbon Accumulation Rates Altered in Soils Undergoing Permafrost Thaw”. In: *Ecosystems* 15.1, pp. 162–173. ISSN: 14329840. DOI: [10.1007/s10021-011-9500-4](https://doi.org/10.1007/s10021-011-9500-4).
- Rampton, V. N. (1987). *Tuktoyaktuk Coastlands, District of Mackenzie, Northwest Territories*. DOI: <https://doi.org/10.4095/125160>.
- (1988). *Quaternary Geology of the Tuktoyaktuk Coastlands, Northwest Territories*. Tech. rep. Memoir 423, pp. 1–107. DOI: [10.1126/science.ns-6.149S.521-a](https://doi.org/10.1126/science.ns-6.149S.521-a).
- Reimer, P. J. et al. (2013). “IntCal13 and Marine13 Radiocarbon Age Calibration Curves 0–50,000 Years cal BP”. In: *Radiocarbon* 55.4, pp. 1869–1887. ISSN: 0033-8222. DOI: [10.2458/azu\\_js\\_rc.55.16947](https://doi.org/10.2458/azu_js_rc.55.16947).
- Repo, M. E., S. Susiluoto, Saara E. Lind, Simo Jokinen, Vladimir Elsakov, Christina Biasi, Tarmo Virtanen, and Pertti J. Martikainen (2009). “Large N<sup>2</sup>O emissions from cryoturbated peat soil in tundra”. In: *Nature Geoscience* 2.3, pp. 189–192. ISSN: 17520894. DOI: [10.1038/ngeo434](https://doi.org/10.1038/ngeo434).
- Romanovsky, V. E., K. Isaksen, D. Drozdov, O. Anisimov, A. Instanes, M Leibman, A. D. McGuire, N. Shiklomanov, S. Smith, and D. Walker (2017).

- “Changing permafrost and its impacts”. In: *Snow, Water, Ice and Permafrost in the Arctic (SWIPA)* 2017, pp. 65–102.
- Romanovsky, V. E., S. L. Smith, and H. H. Christiansen (2010a). “Permafrost thermal state in the polar northern hemisphere during the international polar year 2007-2009: A synthesis”. In: *Permafrost and Periglacial Processes* 21.2, pp. 106–116. DOI: [10.1002/ppp.689](https://doi.org/10.1002/ppp.689).
- Romanovsky, V. E. et al. (2010b). “Thermal state of permafrost in Russia”. In: *Permafrost and Periglacial Processes* 21.2, pp. 136–155. DOI: [10.1002/ppp.683](https://doi.org/10.1002/ppp.683).
- Schaefer, K., T. Zhang, L. Bruhwiler, and A. P. Barrett (2011). “Amount and timing of permafrost carbon release in response to climate warming”. In: *Tellus, Series B: Chemical and Physical Meteorology* 63.2, pp. 165–180. ISSN: 02806509. DOI: [10.1111/j.1600-0889.2011.00527.x](https://doi.org/10.1111/j.1600-0889.2011.00527.x).
- Schuh, Carina, Andrew Frampton, and Hanne Hvidtfeldt Christiansen (2017). “Soil moisture redistribution and its effect on inter-annual active layer temperature and thickness variations in a dry loess terrace in Adventdalen, Svalbard”. In: *Cryosphere* 11.1, pp. 635–651. ISSN: 19940424. DOI: [10.5194/tc-11-635-2017](https://doi.org/10.5194/tc-11-635-2017).
- Schuur, E. A. G. et al. (2015). “Climate change and the permafrost carbon feedback”. In: *Nature* 520.7546, pp. 171–179. ISSN: 14764687. DOI: [10.1038/nature14338](https://doi.org/10.1038/nature14338). arXiv: [arXiv:1011.1669v3](https://arxiv.org/abs/1011.1669v3).
- Shaver, G. R., W. D. Billings, F. S. Chapin, A. E. Giblin, K. J. Nadelhoffer, W. C. Oechel, and E. B. Rastetter (1992). “Global Change and the Carbon Balance of Arctic Ecosystems”. In: *BioScience* 42.6, pp. 433–441. ISSN: 00063568. DOI: [10.2307/1311862](https://doi.org/10.2307/1311862).
- Shiklomanov, N., F. Nelson, D. Streletskiy, and B. K. Biskaborn (2016). “Long-term active-layer dynamics: results of 22 years of field observations in Northern Hemisphere permafrost regions”. In: *Agu 2016*.
- Shur, Y. L. and M. T. Jorgenson (2007). “Patterns of Permafrost Formation and Degradation in Relation to Climate and Ecosystems”. In: *Permafrost and periglacial processes* 18.1, pp. 7–19. DOI: [10.1002/ppp](https://doi.org/10.1002/ppp).
- Sollins, P., G. Spycher, and C. A. Glassman (1984). “Net nitrogen mineralization from light- and heavy-fraction forest soil organic matter”. In: *Soil Biology and Biochemistry*. ISSN: 00380717. DOI: [10.1016/0038-0717\(84\)90122-6](https://doi.org/10.1016/0038-0717(84)90122-6).
- Stevenson, F. J. (1994). *Humus chemistry: genesis, composition, reactions*. John Wiley & Sons.
- Strauss, J. (2010). “Late Quaternary environmental dynamics at the Duvanny Yar key section, Lower Kolyma, East Siberia”. PhD thesis, p. 121.

- Strauss, J. (2014). “Organic carbon in ice-rich permafrost : Characteristics, quantity, and availability” . In:
- Strauss, J. et al. (2017). “Deep Yedoma permafrost: A synthesis of depositional characteristics and carbon vulnerability” . In: *Earth-Science Reviews* 172, pp. 75–86. ISSN: 00128252. DOI: [10.1016/j.earscirev.2017.07.007](https://doi.org/10.1016/j.earscirev.2017.07.007).
- Stuiver, M. and H. A. Polach (1977). “Discussion Reporting of 14 C Data”. In: *Radiocarbon* 19.3, pp. 355–363. DOI: [10.1017/s0033822200003672](https://doi.org/10.1017/s0033822200003672).
- Tamocai, C., J. G. Canadell, E. A. G. Schuur, P. Kuhry, G. Mazhitova, and S. Zimov (2009). “Soil organic carbon pools in the northern circumpolar permafrost region”. In: *Global Biogeochemical Cycles* 23.2, pp. 1–11. ISSN: 08866236. DOI: [10.1029/2008GB003327](https://doi.org/10.1029/2008GB003327).
- Tarnocai, C. (1972). “Some Characteristics of Cryic Organic Soils in Northern Manitoba”. In: *Canadian Journal of Soil Science* 52.3, pp. 485–496. ISSN: 0008-4271. DOI: [10.4141/cjss72-060](https://doi.org/10.4141/cjss72-060).
- Tarnocai, C. and J. G. Bockheim (2011). “Cryosolic soils of Canada: Genesis, distribution, and classification”. In: *Canadian Journal of Soil Science* 91.5, pp. 749–762. ISSN: 0008-4271. DOI: [10.4141/cjss10020](https://doi.org/10.4141/cjss10020).
- Tarnocai, C. and C. Smith (1992). “The formation and properties of soils in the permafrost regions of Canada”. In: *Cryosols: The effects of cryogenesis on the processes and peculiarities of soil formation*. Vol. 1016, pp. 21–42.
- Turetsky, M. R. et al. (2019). *Permafrost collapse is accelerating carbon release*. DOI: [10.1038/d41586-019-01313-4](https://doi.org/10.1038/d41586-019-01313-4).
- Vandenberghe, J. (2013). *Cryoturbation Structures*. 2nd ed. Vol. 3. Elsevier B.V., pp. 430–435. ISBN: 9780444536433. DOI: [10.1016/B978-0-444-53643-3.00096-0](https://doi.org/10.1016/B978-0-444-53643-3.00096-0).
- Vardy, S. R., B. G. Warner, and R. Aravena (1998). “Holocene climate and the development of a subarctic peatland near Inuvik, Northwest Territories, Canada”. In: *Climate Change* 40.2, pp. 285–313.
- Vardy, S. R., B. G. Warner, J. Turunen, and R. Aravena (2000). “Carbon accumulation in permafrost peatlands in the Northwest Territories and Nunavut, Canada”. In: *Holocene* 10.2, pp. 273–280. ISSN: 09596836. DOI: [10.1191/095968300671749538](https://doi.org/10.1191/095968300671749538).
- Vonk, J. E. et al. (2015). *Reviews and Syntheses: Effects of permafrost thaw on arctic aquatic ecosystems*. DOI: [10.5194/bgd-12-10719-2015](https://doi.org/10.5194/bgd-12-10719-2015).
- Walthert, L., S. Zimmermann, P. Blaser, J. Luster, and P. Lüscher (2004). *Waldböden der Schweiz. Band 1 Grundlagen und Region Jura*. hep-Verlag, p. 847. ISBN: 978-3-7225-0070-6.
- Wang, B., B. Paudel, and H. Li (2009). “Retgression characteristics of landslides in fine-grained permafrost soils, Mackenzie Valley, Canada”. In: *Land-*

*slides* 6.2, pp. 121–127. ISSN: 1612510X. DOI: [10.1007/s10346-009-0150-y](https://doi.org/10.1007/s10346-009-0150-y).

Weintraub, M. N. and J. P. Schimel (2005). “Nitrogen Cycling and the Spread of Shrubs Control Changes in the Carbon Balance of Arctic Tundra Ecosystems”. In: *BioScience* 55.5, p. 408. ISSN: 0006-3568. DOI: [10.1641/0006-3568\(2005\)055\[0408:ncatso\]2.0.co;2](https://doi.org/10.1641/0006-3568(2005)055[0408:ncatso]2.0.co;2).

Zhang, T. and K. Stamnes (1998). “Impact of climatic factors on the active layer and permafrost at Barrow, Alaska”. In: *Permafrost and Periglacial Processes* 9.3, pp. 229–246. ISSN: 10456740. DOI: [10.1002/\(sici\)1099-1530\(199807/09\)9:3<229::aid-ppp286>3.0.co;2-t](https://doi.org/10.1002/(sici)1099-1530(199807/09)9:3<229::aid-ppp286>3.0.co;2-t).

## 8 Appendix

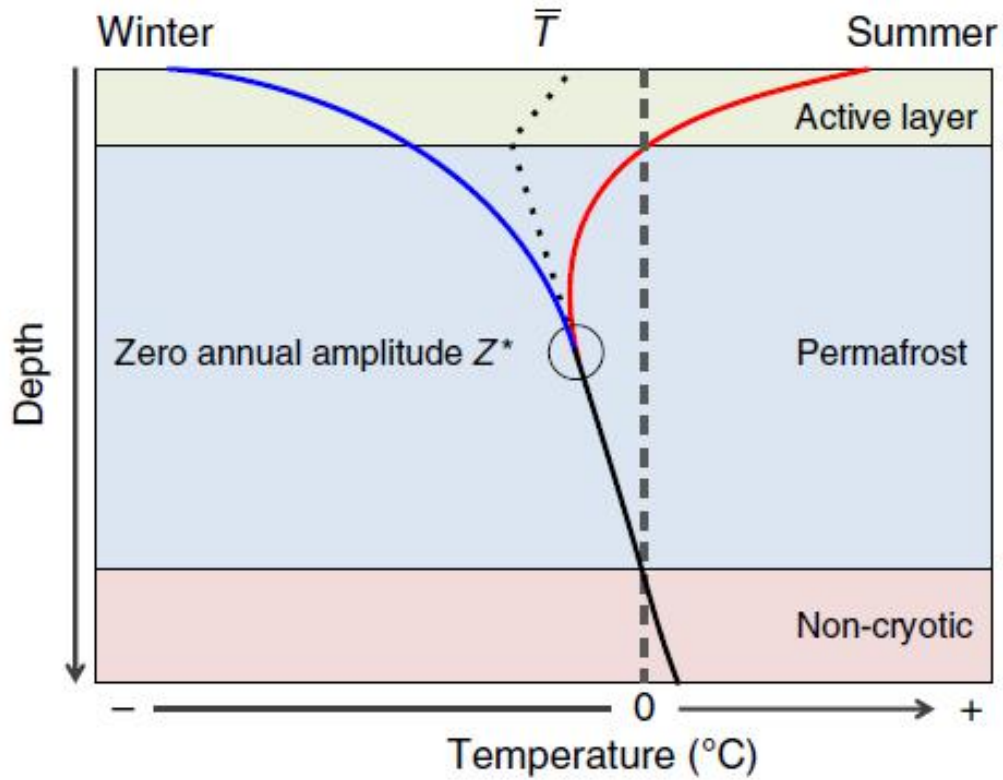


Figure A1: General temperature regime of permafrost from permafrost base to table according to French 2013. Although the minimum permafrost temperatures, the depth of permafrost and the ALT vary across the globe, the general structure remains.

Table A1: Biochemical parameters analysed for the thesis with their according layer boundaries. TN - Total nitrogen, TC - Total carbon, TOC - Total organic carbon, C/N-ratio - Total carbon to total nitrogen ratio.

Position	Upper depth [cm]	Lower Depth [cm]	ALT [cm]	TN [wt%]	TC [wt%]	TOC [wt%]	C/N ratio
L1 Pos1	50	52.5	50	5.75	146.76	153.23	27
L1 Pos1	93	94	50	1.49	21.21	20.04	13
L1 Pos1	63	64.5	50	3.69	92.44	72.59	20
L1 Pos1	60.5	63	50	3.85	104.19	80.3	21
L1 Pos1	66	70.5	50	3.56	99.59	84.61	24
L1 Pos1	70	73	50	2.18	56.2	57.79	27
L1 Pos1	73	76.5	50	4.4	119.41	105.7	24
L1 Pos1	76.5	79.5	50	14.07	333.51	299.95	21
L1 Pos1	79.5	82.5	50	2.94	81.93	79.41	27
L1 Pos2	32	35.5	32	3.1	89.33	71.82	23
L1 Pos2	35	39	32	4.13	142.12	143.89	35
L1 Pos2	43	47	32	5.12	200.04	183.88	36

Position	Upper depth [cm]	Lower Depth [cm]	ALT [cm]	TN [wt%]	TC [wt%]	TOC [wt%]	C/N ratio
L1 Pos2	47	52	32	5.2	131.75	NA	NA
L1 Pos2	62.5	65.5	32	1	20.56	16.61	17
L1 Pos2	73	76.5	32	8.7	244.34	226.66	26
L6 Pos1	50	57	50	2.52	47.44	47.2	19
L6 Pos1	50	58	50	3.21	65.08	53.4	17
L6 Pos2	50	52	50	1	17.98	12.21	12
L6 Pos2	62	65	50	1.08	19.41	16.67	15
L6 Pos2	65	70	50	1.94	35.14	35.09	18
L6 Pos2	70	75.5	50	5.02	104.33	73.81	15
1sub3	85	95	85	1	14.24	10.51	11
1sub3	98.5	101	85	1	13.18	9.45	9
1sub3	107.5	109.5	85	1	14.09	9.24	9
TVC	45	49	45	1	6.64	4.23	4
L11 Pos6	0	30	73	1.35	29.04	25.36	19
L11 Pos6	40	46	73	1	15.39	11.97	12
L11 Pos4	0	10	95	1.3	23.61	19.81	15
L11 Pos4	10	20	95	1.2	22.21	19.63	16
L11 Pos4	20	30	95	1.13	19.99	17.6	16
L11 Pos4	30	40	95	1.2	20.95	19.51	16
L11 Pos4	40	50	95	1.4	25.81	22.36	16
L11 Pos4	50	70	95	1.07	21.19	17.37	16
L11 Pos4	70	90	95	1	17.9	12.8	13
L11 Sim	0	10	98	1.59	27.71	23.75	15
L11 Sim	10	30	98	1.81	34.75	34.07	19
L11 Sim	30	50	98	2.32	43.43	42.49	18
L11 Sim	50	70	98	1.16	19.96	17.25	15
L11 Sim	70	100	98	1	14.32	10.22	10
L6 Pos1	NA	NA	50	2.21	45.88	42.03	19
L12 Pos2	20	30	74.5	1.03	17.09	13	13
L12 Pos2	50	60	74.5	1	15.94	10.6	11
L12 Pos3	5	20	87	2.36	55.33	49.6	21
L12 Pos3	20	30	87	1.22	27.46	23.63	19
L12 Pos3	40	50	87	1.51	28.89	25.15	17
L12 Pos3	70	80	87	1	15.13	10.16	10
L12 Pos5	20	30	100	1.01	16.12	12	12
L12 Pos5	70	80	100	1	15.41	10.63	11
L12 Sim	0	10	96	1	12.96	8.67	9
L12 Sim	10	30	96	1	12.35	8.1	8

Position	Upper depth [cm]	Lower Depth [cm]	ALT [cm]	TN [wt%]	TC [wt%]	TOC [wt%]	C/N ratio
L12 Sim	30	50	96	1	12.46	8.86	9
L12 Sim	50	70	96	1	14.51	9.22	9
L12 Sim	70	90	96	1	14.89	9.63	10
L12 Sim	90	100	96	1	16.01	9.8	10
1sub3	0	10	85	1.02	16.79	13.63	13
1sub3	20	30	85	1.59	29.33	26.1	16
1sub3	50	60	85	1.78	32.64	31.85	18

*Table A1: Grain size distribution of all measured sites. Sorted alphabetically and according to the upper depth. no - undisturbed, yes - disturbed, L - Lake, NA - not available.*

Position	Upper Depth [cm]	Lower Depth [cm]	ALT [cm]	Distur- bance	Sand fraction	Silt fraction	Clay fraction
1sub3	0	10	85	no	0.204	0.605	0.182
1sub3	20	30	85	no	0.209	0.601	0.19
1sub3	50	60	85	no	0.23	0.59	0.18
1sub3	85	95	85	no	0.172	0.644	0.184
1sub3	98.5	101	85	no	0.193	0.607	0.2
1sub3	107.5	109.5	85	no	0.195	0.616	0.189
L1 Pos1	50	52.5	50	no	0.095	0.634	0.266
L1 Pos1	60.5	63	50	no	0.303	0.469	0.195
L1 Pos1	63	64.5	50	no	0.127	0.631	0.231
L1 Pos1	66	70.5	50	no	0.189	0.556	0.232
L1 Pos1	70	73	50	no	0.221	0.562	0.195
L1 Pos1	73	76.5	50	no	0.131	0.621	0.246
L1 Pos1	76.5	79.5	50	no	0.107	0.711	0.172
L1 Pos1	79.5	82.5	50	no	0.249	0.579	0.172
L1 Pos1	93	94	50	no	0.177	0.567	0.256
L1 Pos2	32	35.5	32	no	0.138	0.64	0.209
L1 Pos2	35	39	32	no	0.193	0.593	0.192
L1 Pos2	43	47	32	no	0.162	0.662	0.176
L1 Pos2	47	52	32	no	0.285	0.559	0.155
L1 Pos2	62.5	65.5	32	no	0.176	0.644	0.179
L1 Pos2	73	76.5	32	no	0.138	0.614	0.238
L1 Pos2	80	90	32	no	0.408	0.422	0.147
L11 Pos4	0	10	95	yes	0.238	0.576	0.186
L11 Pos4	10	20	95	yes	0.309	0.534	0.153
L11 Pos4	20	30	95	yes	0.252	0.582	0.166

Position	Upper Depth [cm]	Lower Depth [cm]	ALT [cm]	Distur- bance	Sand fraction	Silt fraction	Clay fraction
L11 Pos4	30	40	95	yes	0.187	0.636	0.177
L11 Pos4	40	50	95	yes	0.213	0.599	0.188
L11 Pos4	50	70	95	yes	0.219	0.538	0.238
L11 Pos4	70	90	95	yes	0.212	0.591	0.193
L11 Pos6	0	30	73	no	0.271	0.584	0.145
L11 Pos6	40	46	73	no	0.363	0.509	0.128
L11 Sim	0	10	98	yes	0.239	0.585	0.176
L11 Sim	10	30	98	yes	0.244	0.595	0.161
L11 Sim	30	50	98	yes	0.239	0.59	0.171
L11 Sim	50	70	98	yes	0.179	0.633	0.189
L11 Sim	70	100	98	yes	0.143	0.668	0.189
L12 Pos2	20	30	74.5	yes	0.174	0.629	0.196
L12 Pos2	50	60	74.5	yes	0.169	0.649	0.182
L12 Pos3	5	20	87	yes	0.241	0.608	0.151
L12 Pos3	20	30	87	yes	0.158	0.656	0.186
L12 Pos3	40	50	87	yes	0.148	0.663	0.189
L12 Pos3	70	80	87	yes	0.153	0.679	0.168
L12 Pos5	20	30	100	yes	0.213	0.61	0.177
L12 Pos5	70	80	100	yes	0.18	0.644	0.175
L12 Sim	0	10	96	yes	0.22	0.617	0.164
L12 Sim	10	30	96	yes	0.245	0.591	0.163
L12 Sim	30	50	96	yes	0.166	0.644	0.19
L12 Sim	50	70	96	yes	0.134	0.668	0.198
L12 Sim	70	90	96	yes	0.16	0.644	0.196
L12 Sim	90	100	96	yes	0.183	0.661	0.156
L6 Pos1	50	58	50	no	0.182	0.675	0.143
L6 Pos1	NA	NA	50	no	0.258	0.614	0.128
L6 Pos2	50	52	50	yes	0.027	0.743	0.23
L6 Pos2	62	65	50	yes	0.169	0.628	0.203
L6 Pos2	65	70	50	yes	0.26	0.582	0.158
L6 Pos2	70	75.5	50	yes	0.197	0.651	0.14
TVC	45	49	45	no	0.457	0.478	0.065

Table A1: Error of grain size analysis method. Table showing the sites with their associated layer boundaries, measurement of grains larger 1mm of the laser grain size analyser, excluded grains larger 1mm and included grains smaller 1mm (see Chapter 2.3.2 and 2.4). Sites without any grains larger 1mm were excluded from this table.

Site Position	Depthup [cm]	Depthdown [cm]	Error Laser >1mm [vol%]	Grains >1mm [wt%]	Grains <1mm [wt%]
L1 Pos1	50	52.5	2.07	0.44	99.5
L1 Pos1	93	94	0	1.28	98.72
L1 Pos1	63	64.5	4.49	0.01	99.99
L1 Pos1	60.5	63	12.74	0.33	99.67
L1 Pos1	66	70.5	8.85	0.33	99.67
L1 Pos1	70	73	8.19	9.30	90.70
L1 Pos1	73	76.5	1.14	0.78	99.22
L1 Pos1	76.5	79.5	3.86	2.73	97.27
L1 Pos1	79.5	82.5	0	1.33	98.67
L1 Pos2	32	35.5	4.93	1.62	98.38
L1 Pos2	47	52	2.36	4.94	95.06
L1 Pos2	62.5	65.5	1.84	1.14	98.86
L1 Pos2	80	90	10.11	1.28	98.72
L6 Pos1	50	58	0	0.35	99.65
L6 Pos2	50	52	0	1.92	98.08
L6 Pos2	65	70	.64	1.21	98.79
L6 Pos2	70	75.5	5.12	0.14	99.86
L6 Pos1	na	na	25.76	0.28	99.72
1sub3	85	95	0.29	0.42	99.58
1sub3	98.5	101	0.67	5.89	94.11
1sub3	0	10	20.44	0.36	99.64
1sub3	20	30	20.86	0.72	99.28
L11 Pos6	0	30	0	0.1	99.9
L11 Pos6	40	46	0	0.67	99.33
L11 Pos4	0	10	0	0.38	99.62
L11 Pos4	10	20	4.09	0.94	99.06
L11 Pos4	20	30	0	0.47	99.53
L11 Pos4	30	40	0	0.55	99.45
L11 Pos4	40	50	0	0.82	99.18
L11 Pos4	50	70	2.26	0.10	99.90
L11 Pos4	70	90	1.81	0.18	99.82
L11 Sim	10	30	0.10	0.54	99.46
L11 Sim	30	50	0	0.75	99.25
L11 Sim	0	10	22.00	1.41	98.59

Site Position	Depthup [cm]	Depthdown [cm]	Error Laser >1mm [vol%]	Grains >1mm [wt%]	Grains <1mm [wt%]
L11 Sim	10	30	24.53	0.23	99.77
L11 Sim	30	50	16.62	0.15	99.85
L12 Pos2	20	30	17.44	1.14	98.86
L12 Pos2	50	60	16.88	0.72	99.28
L12 Pos3	5	20	24.14	0.22	99.78
L12 Pos3	20	30	15.76	3.71	96.29
L12 Pos3	40	50	14.78	0.53	99.47
L12 Pos3	70	80	15.30	0.16	99.84
L12 Pos5	20	30	21.31	1.04	98.96
L12 Pos5	70	80	18.02	1.45	98.55

*Table A1: ALT measurements by Inge Grünberg, AWI during the same expedition to NWT, Canada. Some sites appear only in this table since the number of ALT measurements exceed those of sites otherwise included in this thesis. NA = Not Available, L = Lake, yes = disturbed, no = undisturbed, NA - not available.*

Position	Longitude [dec°]	Latitude [dec°]	Mean ALT [cm]	Disturbance category
Bare 1	-133.51919564	68.74517961	100	yes
Bare 2	-133.52347871	68.74544691	87.3	yes
Dwarf shrub 1	-133.50340609	68.74316695	na	no
Dwarf shrub 2	-133.50671131	68.74350633	64.3	no
Dwarf shrub 3	-133.52424895	68.74511286	62	no
Forest 1	-133.51715478	68.74289403	36.6	no
High centered polygon 1	-133.54063742	68.74976338	na	no
High centered polygon 2	-133.54026043	68.7499885	43	no
High centered polygon 3	-133.53982931	68.74995906	36	no
Lake1 1	-133.73379224	68.57559104	59	no
Lake1 3	-133.73379224	68.57559104	73	no
Lake11 1	-133.46536964	68.75457362	100	yes
Lake11 2	-133.46522599	68.7544562	93	yes
Lake11 3	-133.46509164	68.75423074	70	yes
Lake11 4	-133.46513906	68.75394413	95	yes
Lake11 5	-133.46508443	68.75378851	76	no
Lake11 6	-133.46507615	68.75363717	73	no
Lake11 ref 1	-133.46929584	68.75500587	45	NA
Lake11 ref 2	-133.46937029	68.75495726	48	no
Lake11 ref 3	-133.46989451	68.75475987	62	no

Position	Longitude [dec°]	Latitude [dec°]	Mean ALT [cm]	Disturbance category
Lake12 1	-133.51950241	68.75761533	93	no
Lake12 2	-133.51954413	68.75766011	74.5	yes
Lake12 3	-133.51970507	68.75792797	87	yes
Lake12 4	-133.52024158	68.75832531	98	yes
Lake12 5	-133.52037244	68.75859378	98	yes
Lake12 6	-133.51930151	68.75745294	80	no
Lake12 ref 1	-133.51833964	68.75843722	29	no
Lake12 ref 2	-133.51820528	68.75835725	41	no
Lake6 1	-133.25362601	69.03373989	32.7	no
Lake6 2	-133.2536655	69.03365104	35	no
Lake6 3	-133.25375235	69.03353396	35	no
Lake6 4	-133.2537567	69.03345109	38	no
Lake6 5	-133.25382485	69.03335437	35	no
Lake6 6	-133.25388306	69.03325784	65	no
Lake6 7	-133.25391468	69.03322036	70	yes
Lake6 8	-133.25405886	69.03314565	100	yes
Lake6 9	-133.25422213	69.03297261	100	yes
Lake6 10	-133.25434872	69.03283301	82	yes
Lake6 ref 1	-133.25588895	69.03309435	100	no
Lake6 ref 2	-133.25568671	69.03317569	26.3	no
Lichen 1	-133.51188223	68.74361115	76	no
Lichen 2	-133.51915552	68.74494644	75.7	no
Polygon rim 1	-133.54044048	68.74973913	48.7	NA
Polygon rim 2	-133.54076175	68.74986649	62	NA
Riparian shrub 0	-133.51144852	68.74387341	47	NA
Riparian shrub 1	-133.51441487	68.7419832	60	NA
Riparian shrub 2	-133.51645395	68.74168324	32.3	NA
Riparian shrub 3	-133.51773101	68.74224892	61.75	NA
Riparian shrub 4	-133.51984826	68.74466029	86.3	NA
Tall shrub 1	-133.52118374	68.74572783	56.7	no
Tussock 1	-133.51653445	68.74197015	54	no
Tussock 2	-133.51745481	68.74241352	37.3	no
Wet sedges 1	-133.52267391	68.74539776	100	yes



Figure A2: Map of sampling setup at Lake 1 regarding the main data set ( $[-133.7338, 68.57559]$ ). Position 1 and 2 are right next to each other and are therefore just represented as one location. Background map is created with an satellite imagery map from 2017 provided by Google (Google Maps 2017).

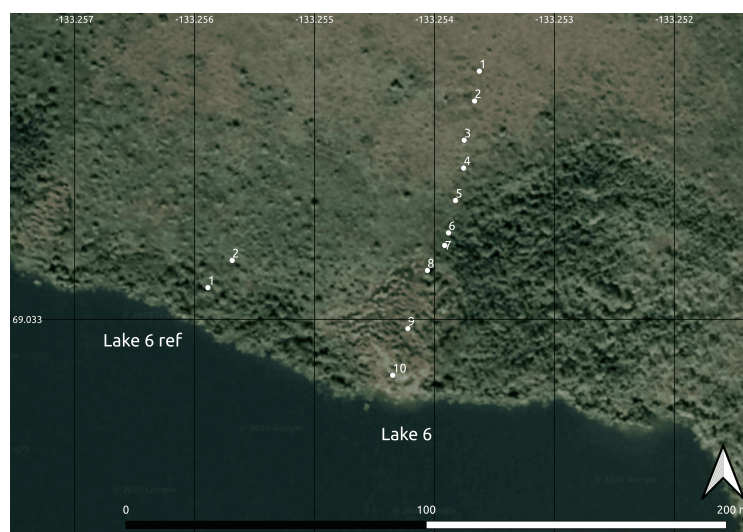


Figure A3: Map of sampling setup at Lake 1 regarding the main data set ( $[-133.2557, 69.03318]$ ). Background map is created with an satellite imagery map from 2017 provided by Google (Google Maps 2017).

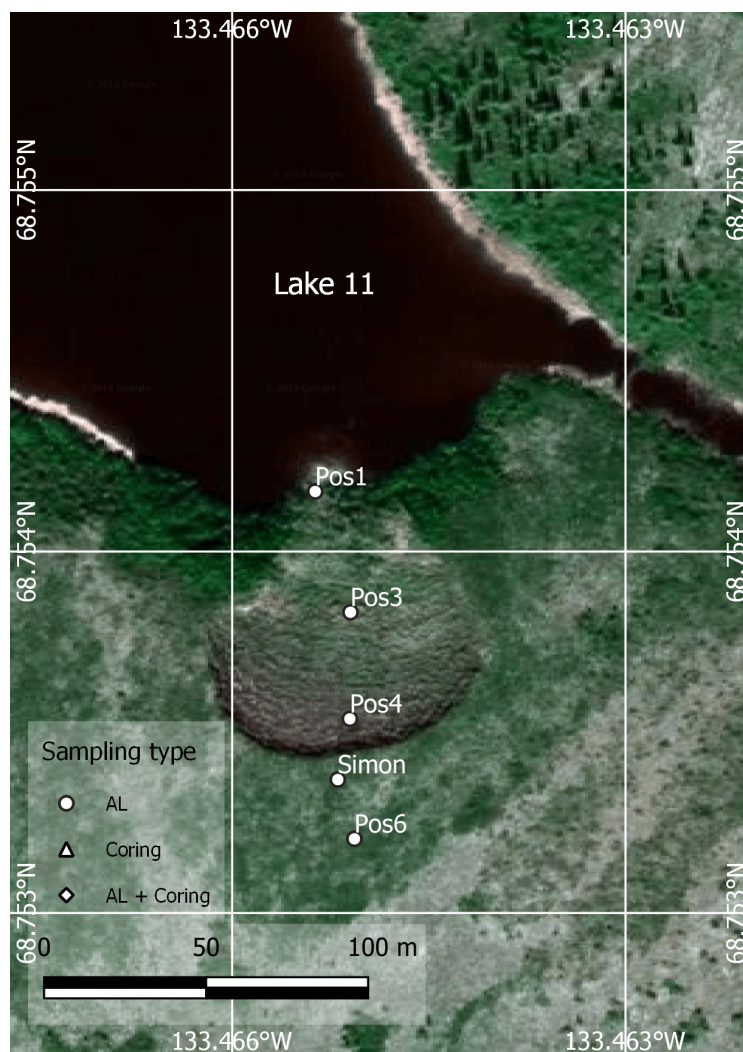


Figure A4: Map of sampling setup at Lake 11 regarding the main data set ( $[-133.4651, 68.75364]$ ). Background map is created with an satellite imagery map from 2017 provided by Google (Google Maps 2017).

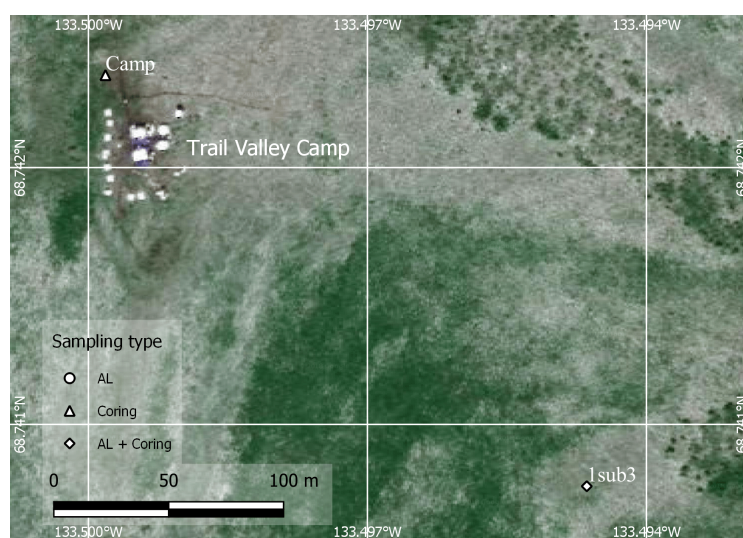


Figure A5: Map of sampling setup at TVC and 1sub3 regarding the main data set (TVC:  $[-133.499617, 68.74236]$ , 1sub3:  $[-133.494441, 68.740759]$ ). Background map is created with an satellite imagery map from 2017 provided by Google (Google Maps 2017).

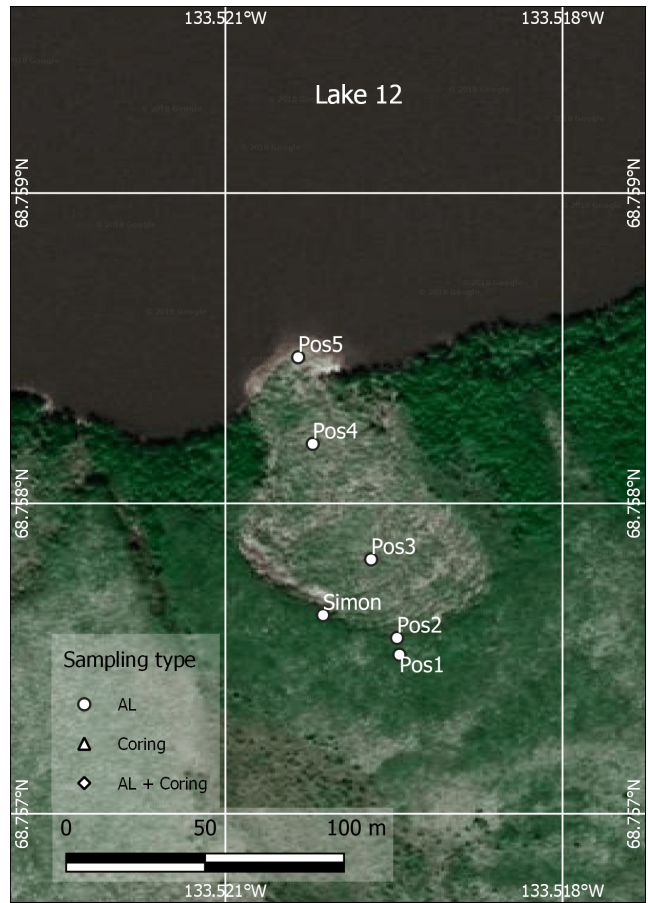


Figure A6: Map of sampling setup at Lake 12 regarding the main data set  $([-133.5193, 68.75745])$ . Background map is created with an satellite imagery map from 2017 provided by Google (Google Maps 2017).



Figure A7: Map of sampling setup at Lake 1 of Inge Grünberg, AWI regarding the extended data set of ALT measurements  $([-133.7338, 68.57559])$ . Position 1 and 3 are right next to each other and are therefore just represented as one location. Background map is created with an satellite imagery map from 2017 provided by Google (Google Maps 2017).



Figure A8: Map of sampling setup at Lake 6 of Inge Grünberg, AWI regarding the extended data set of ALT measurements  $([-133.2557, 69.03318])$ . Background map is created with an satellite imagery map from 2017 provided by Google (Google Maps 2017).



Figure A9: Map of sampling setup at Lake 11 of Inge Grünberg, AWI regarding the extended data set of ALT measurements  $([-133.4651, 68.75364])$ . Background map is created with an satellite imagery map from 2017 provided by Google (Google Maps 2017).

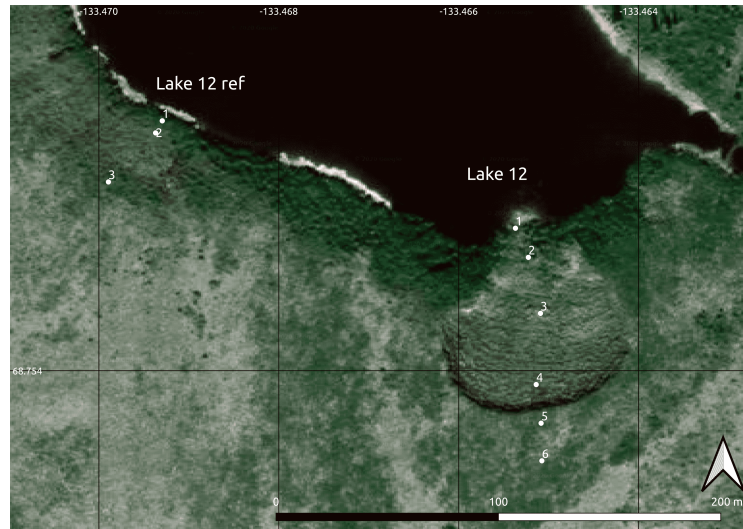


Figure A10: Map of sampling setup at Lake 12 of Inge Grünberg, AWI regarding the extended data set of ALT measurements (-133.5193,68.75745). Background map is created with an satellite imagery map from 2017 provided by Google (Google Maps 2017).



Figure A11: Sample setup of vegetation sites of Inge Grünberg, AWI close to TVC regarding the extended data set of ALT measurements ([-133.4651,68.75364]). Background map is created with an satellite imagery map from 2017 provided by Google (Google Maps 2017).